A Study of Molecular- and Meso- Tin Sulfides

by

Ömer Kardeş Yükseker

A thesis submitted in conformity with the requirements

for the Degree of Master of Science in the

Graduate Department of Chemistry,

University of Toronto

© Copyright by Ömer Kardeş Yükseker 2001

National Library of Canada
Acquisitions and Bibliographic Services
395 Wellington Street
Ottawa ON K1A 0N4
Canada

Bibliothèque nationale du Canada
Acquisitions et services bibliographiques
395, rue Wellington
Ottawa ON K1A 0N4
Canada

Your file Votre référence

Our file Notre référence

The author has granted a non-exclusive licence allowing the National Library of Canada to reproduce, loan, distribute or sell copies of this thesis in microform, paper or electronic formats.

L'auteur a accordé une licence non exclusive permettant à la Bibliothèque nationale du Canada de reproduire, prêter, distribuer ou vendre des copies de cette thèse sous la forme de microfiche/film, de reproduction sur papier ou sur format électronique.

The author retains ownership of the copyright in this thesis. Neither the thesis nor substantial extracts from it may be printed or otherwise reproduced without the author's permission.

L'auteur conserve la propriété du droit d'auteur qui protège cette thèse. Ni la thèse ni des extraits substantiels de celle-ci ne doivent être imprimés ou autrement reproduits sans son autorisation.

0-612-58763-0

Canada

"A Study of Molecular- and Meso- Tin Sulfides", by Ömer Kardeş Yükseker, Master's Thesis, Department of Chemistry, University of Toronto, 2001

Abstract

A brief overview of tin sulfides – from molecules to three dimensional frameworks – is presented. The section on molecular tin sulfides begins with the structure of the $TMA_4Sn_4S_{10}$ tetramer. The pH dependent interconversion of the SnS_4^{4-} monomer to the $Sn_2S_6^{4-}$ dimer and vice versa is explored using ^{119}Sn aqueous phase NMR. Switching to meso tin sulfides, a set of new materials templated by long-chain amines are examined using powder x-ray diffraction. The thermotropic liquid crystal behaviour of the tetradecylammonium templated material is confirmed by differential scanning calorimetry. Structural parameters, most successfully tin-sulfur distances, are obtained for this material by studying the extended x-ray absorption fine structure (EXAFS) imposed on its x-ray absorption spectrum near the K-edge of tin. Also included is a brief overview of the theory of EXAFS and data analysis using this data.

Acknowledgments

Thank you,

First of all, to Geoff, without whom I would not have had a chance to write this

Next, to my parents, who form the bedrock of who I am

My colleagues, for their help and understanding

To my family, friends, for making everything worth while

Table of Contents

List of Tables

Chapter 3 – Search for the Tin Sulfide Tetramer

Chapter 5 – An EXAFS Study of Meso Tin Sulfides

List of Figures

Chapter 3 – Search for the Tin Sulfide Tetramer

Chapter 4 – New Meso Tin Sulfides

Chapter 5 – An EXAFS Study of Meso Tin Sulfides

Chapter 1 – Introduction

Recently a very interesting article[1] appeared as one of *Nature*'s millennium essays. In that article Gautam R. Desiraju observed that chemistry, unlike any other science, has developed under the influence of one thinker, Linus Pauling. He points out that for much of our field's history Pauling's 'grand unification of molecular structure' has provided the framework for chemical research. A potential consequence, he suggests, is that chemistry has been locked out of differing avenues of thought. He contrasts chemistry with physics and biology and points out they possess much greater diversity. This is not a criticism of chemistry. Rather is a statement about the concept of the molecule proving to be incredibly fruitful.

Mr. Desiraju does not stop with this observation, however. He goes on to state that chemistry today is undergoing a metamorphosis, breaking out of the dominance of the molecule. In the fertile grounds where chemistry is meeting biology and materials science a new complexity is emerging. Here are fields that contain systems of great interdependence, timescales of ever shorter duration and length scales spanning many more orders of magnitude.

This then, is the new face of chemistry. The molecule no longer is the pinnacle, rather, it is the foundation. And because of chemistry's focus to date, it is a very solid foundation indeed.

It is fortunate for me, then, that I had the opportunity to study chemistry at this point in history, and doubly fortunate that this took place in a materials chemistry lab. Willingly or unwillingly, this paper traces some of the changes taking place in chemistry. The first chapter reviews tin sulfides, the category under which the rest of the work takes place. In the second chapter work on molecular tin sulfides is covered – the goal of this study was to provide molecular precursors for mesoscale assembly. The third chapter looks at mesoscale materials themselves. It is an extension of previous work in our group on meso tin sulfides. In the final chapter is an EXAFS study of these meso tin sulfides.

Reference

[1] Desiraju, G. R.; *Nature* 408, 407, **2000**

Chapter 2 – A Brief Review of Tin Sulfide Materials

Tin sulfides can be found in compounds ranging from molecular species to three-dimensional materials. What follows is an overview of these materials. What should be kept in mind is that there is a great variety of structures and motifs. This is one of the great potentials offered by working with tin, which can be very versatile in its bonding character.

2.1 Tin Sulfide Molecules

Inevitably, the molecular species have four coordinate tin, the simplest of which is the tetrahedral SnS_4^{4-}. This molecule can be prepared by a solid state synthesis[1] and from the stochiometric reaction[2] of $SnCl_4$ with an aqueous solution of Na_2S. It is not at all surprising that the high temperature synthesis yields a much denser product (Na_4SnS_4) than the aqueous method ($Na_4SnS_4 \cdot 14H_2O$).

This tetrahedral monomer forms a basic building block for many other tin sulfide materials. For example, the remaining molecular tin sulfides are oligomeric condensation products of this molecule. If sharing a corner joins two of these monomers, the dimeric $Sn_2S_7^{4-}$ is produced, as reported by both Jumas[3] and Krebs[4]. Both investigators prepared the dimer by the high temperature reaction of Na_2S with elemental tin and sulfur.

When two SnS_4^{4-} share an edge rather than a corner another dimeric molecule, $Sn_2S_6^{4-}$ is produced. Krebs[5] has described two room temperature aqueous routes to this molecule. The first is through a 1:1 reaction of SnS_2 and Na_2S, the other through a 3:1 reaction of Na_2S and $SnCl_4$. Both reactions yield highly hydrated sodium salts, with 14 water molecules per dimer. The $Sn_2S_6^{4-}$ dimer has also been isolated from mother liquors of hydrothermal syntheses of SnS-1 and SnS-3 materials (see below). Furthermore, Kessler[6] has produced this dimer with dodeclyamine as the cation. Kessler's molecule crystallizes in a lamellar fashion, with the $Sn_2S_6^{4-}$ in layers, alternating with layers of the surfactant.

Another possible tin sulfide molecule is the adamantane shaped $Sn_4S_{10}^{4-}$ tetramer. This configuration of atoms is possible with many different atoms[7]. Among tin sulfides it can be seen in molecules of the type $R_4Sn_4S_6^{4-}$ molecules[8]. The $Sn_4S_{10}^{4-}$ tetramer itself is described as being 'completely characterized'[9] although no details are to be found in the literature. This lack of attention is interesting, given the intense interest in the germanium counterpart as a building block in metal-linked 3D nanoporous frameworks[10], mesostructured germanium sulfides[11,12] and a new dense GeS_2 phase[13].

In contrast with molecular tin sulfides tin polysulfides are six coordinate. In the two molecules reported[14,15] three polysulfide chains are attached to each tin. These ligands are either S_4^{2-} singly or in combination with S_6^{2-}. These molecules have been isolated with the organic counter ions tetraethylammonium (TEA) or 1,3,5,diaza[1,1,1]bicyclooctane (DABCO). Examples are $TEA_2[Sn(S_4)_3]_{.4}[Sn(S_4)_2S_6]_{.6}$[13] and $DABCOH_2[Sn(S_4)_3]_{.5}[Sn(S_4)_2S_6]_{.5}$[14]. The latter, for example, is prepared by the hydrothermal reaction of the mixture DABCO:Sn:2S:35H_2O at 100 °C.

2.2 Tin Sulfide Polymers

It is easy to imagine that if the condensation of SnS_4^{4-} tetrahedra proceeds past the oligomeric stage, polymeric tin sulfides can be produced. To date, there is one example in the literature[16]. It consists of corner sharing tetrahedra and can be visualized as an infinite chain of $Sn_2S_7^{4-}$ dimers. The material $K_2SnS_3 \cdot 2H_2O$ features parallel chains in which the motif -Sn-S-Sn-S- is repeated. It is synthesized from a basic solution of potassium hydroxide saturated with H_2S to which SnS_2 is added until saturation. This solution is heated to boiling and refluxed for five minutes and allowed to cool while stirring.

2.3 Two Dimensional Tin Sulfides

A great wealth of tin sulfide materials are organized into two dimensional sheets. Chief among these is tin sulfide, SnS_2. As is with many metal chalcogenides of type MX_2, the structure of each SnS_2 sheet consists of a plane of hexagonal six coordinate tin

sandwiched between two sheets of hexagonally arranged three coordinate sulfur. While the intralayer bonding is covalent, van der Waals interactions hold the successive sheets together. The stacking of these layers in SnS_2 is quite diverse, with over 70 polytypes reported[17]. It is quite amazing that in one polytype the stacking sequence repeats every 258 layers to give a unit cell parameter *c* of 761Å[18]! It has recently been proposed that SnS_2 sheets can be viewed as quasi one dimensional molecular crystals and a new labeling scheme has been described for the various polytypes[19].

Currently there is growing interest in the lamellar, dense tin sulfides. SnS_2 is a semiconductor with an indirect band gap that is usually quoted as 2.18 eV[20]. However the band gap depends on layer stacking, and can vary between 0.81 eV and 3.38 eV between the various polytypes[19]. The main interest in SnS_2 is as an intercalation host for lithium ions in rechargeable batteries[21,22].

SnS_2 can be prepared in many different ways. Amorphous SnS_2 is readily obtained from the mixture of stoichiometric amounts of Na_2S and $SnCl_4$ solutions[23]. This synthesis is very useful in producing SnS_2 as a starting material, as it is very easy and the material can be readily washed to remove the chloride contaminant often found in ready-bought SnS_2. Crystalline materials can be made from the elements at high temperature[24]. Synthesis *via* chemical vapour transport (CVT) has been reported by Patel[25]. At atmospheric pressures Parkin was able to deposit films of crystalline SnS, Sn_2S_3 and SnS_2 onto glass substrates from appropriate gas-phase mixtures of H_2S and $SnCl_4$[20]. The advantages of this approach are that it avoids high cost precursors and does not need a CVT chamber. This final point is important as the author envisions incorporating the coating process to the glass production process. In this regard SnS with its direct band gap of 1.4 eV[26] is attractive as a solar energy collector.

Moving away from these dense materials, we come to the microporous nets invented by Bedard. Although sketchily characterized in the original patent, these materials eventually yielded to full analysis[27,2728]. It is interesting that UOP scientists first described both these porous metal sulfides and AlPO's. UOP being a leading figure in the petrochemical industry, it is easy to see their interest in such materials. Here we have materials that combine the porous aspects of zeolites, which give them their extraordinary

abilities in catalysis and their size/shape selectivity, with elements other than silicon, aluminum and oxygen. Of particular interest to the petrochemical industry is the substitution of sulfur for oxygen, with hopes of preventing sulfur poisoning of the catalyst.

Designated SnS-1 and SnS-3 these microporous tin sulfides are layered materials, much like SnS_2. The layer structure and chemical composition are somewhat different. Rather than being pure inorganic materials, SnS-1 and SnS-3 are inorganic/organic hybrids. The inorganic tin sulfide provides the framework while the organic component balances charge, fills space and is structure directing during synthesis.

The building block for both materials is the Sn_3S_4 broken cube. Chemically speaking SnS-1 is $R_2Sn_3S_7$, where R is the organic cation. If the cation is changed from, say TEA or DABCO to tetraproplyammonium (TPA), the resulting material is $R_2Sn_4S_9$, or SnS-3. While the SnS-1 layers are flat, those of SnS-3 are corrugated. The corrugation prevents the larger organic molecules from overlapping each other. In SnS-1 the layers are tiled by Sn_3S_4 broken cubes arranged hexagonally and linked by (μ-S_2) disulfide bridges. This hexagon is elongated into an ellipsoid in the SnS-3 structure and the ring expands from 24 to 32 atoms. Again, there are six broken cubes, but now four of the linkages are through (μ-S_2SnS_2) bridges.

These materials are most readily synthesized from mixtures of tin and sulfur sources under hydrothermal conditions. For example, DABCO-SnS-1 can be made from a mixture of DABCO : Sn : 2 S : $(NH_4)_2S$: 30 H_2O tumbled at 150 °C for one to two days. The same procedure, but with a mixture of TPAOH: Sn : 2 S : 0.5 $(NH_4)_2S$: 160 H_2O yields TPA-SnS-3

The question of whether even larger organic molecules would lead to the formation of newer structures was answered affirmatively with the synthesis of the material designated meso tin sulfide. Compared to SnS-1 and SnS-3, meso tin sulfide is radically different. The organic component is no longer a small cation, but is now a surfactant – hexadecylamine (HDA). Note that this is a neutral molecule which can be positively charged at the correct pH. Similar to other lamellar tin sulfides, this material

also contains distinct tin sulfide layers separated by, in this case, a bilayer of the organic surfactant.

Further interesting differences are revealed as we look in more detail. Initially, the term meso was used to describe this material as it exhibits features in the 50 Å region. This number corresponds to the layer spacing. Actually, this material is "doubly" meso since it is also a mesogen, specifically a thermotropic liquid crystal. The existence of a mesogenic phase was shown using polarized optical microscopy, and the phase transitions followed by differential scanning calorimetry and by variable temperature powder x-ray diffraction. It was shown that heating first leads to a loss of order in the surfactant phase, followed by the loss of order in the tin sulfide layer. Unfortunately this material has not yielded to single crystal diffraction analysis, and the exact nature of the tin sulfide layer remains unresolved. Solid state $^{1}H/^{119}Sn$ CP-MAS spectroscopy has revealed the presence of both five and six coordinate tin.

2.4 Three Dimensional Tin Sulfide Frameworks

Finally, arriving at three dimensional tin sulfide frameworks, we see that there are only two members of this family. Both are prepared *via* solid state synthesis, in sealed tubes at high temperatures. These materials have the chemical formulae of $K_2Sn_2S_5$ and $Na_4Sn_3S_8$.

They both feature rings, of 12 atoms for the former and of 14 atoms for the latter. Although both structures contain large openings in their structure, this void is entirely filled in $K_2Sn_2S_5$ by the charge-balancing K^+ ions, and in the case of the other material by Na^+ ions at sulfur atoms that protrude into the ring.

2.5 References

1. Jumas, J. C.; Vermot-Gaud-Daniel, F.; Phillipot, E. *Cryst. Struct. Comm.* 2, 157, **1973**

2. Krebs, B.; Pohl, S.; Schiwy, W. *Z. Anorg. Allg. Chem.* 398, 63-71, **1973**

3. Jumas, J. C.; Olivier-Fourcade, J.; Vermot-Gaud-Daniel, F.; Ribes, M.; Phillipot, E.; Maurin, M. *Rev. Chim. Mineral*

4. Krebs, B.; Pohl, S.; Schiwy, W. *Z. Anorg. Allg. Chem.* 398, 63-71, **1973**

5. Krebs, B.; Pohl, S.; Schiwy, W. *Z. Anorg. Allg. Chem.* 393, 241-252, **1972**

6. Li, J.; Marler, B.; Kessler, H.; Soulard, M.; Kallus, S. *Inorg Chem.* 36, 4697-4701, **1997**

7. Vittal, J. J.; *Polyhedron.* 15, 1585-1642, **1996**

8. Smith, P. J. , Ed. *Chemistry of Tin, 2nd Edition*.. Chapman, Hall, London 1998, p. 46

9. Krebs, B. *Angew. Chem. Int. Ed. Engl.* 22, 113-134, **1983**

10. Bowes, C. L.; Huynh, W. U.; Kirkby, S. J.; Malek, A.; Ozin, G. A.; Petrov, S.; Twardoski, M.; Young, D.; Bedard, R. L., Broach, R. *Chem. Mater.* 8, 2147-2152, **1996**

11. MacLachlan, M. J.; Coombs, N.; Bedard, R. L.; White, S.; Thompson, L. K.; Ozin, G. A. *J. Am. Chem. Soc.* 121, 12005-12017, **1999**

12. Bonhomme, F.; Kanatzidis, M. G. *Chem. Mater.* 10, 1153-1159, **1998**

13. MacLachlan, M. J.; Petrov, S.; Bedard, R. L.; Manners, I.; Ozin, G. A. *Angew. Chem. Int. Ed. Engl.* 37, 2076-2079, **1998**

14. Muller, A.; Schimanski, J.; Romer, M.; Bogge, H.; Baumann, W.; Elzner, W.; Kreckemeyer, E.; Bellerbeck, U. *Chimia.* 39, 25, **1985**

15. Jiang, T.; Ozin, G. A.; Bedard R. L. *Adv. Mater.* 6, 860, **1994**

16. Schivy, W.; Blutau, C.; Gäthje, D.; Krebs, B.. *Anorg. Allg. Chem.* 412, 1-96, **1975**

17. Polosz, B.; Steurer, W.; Schatz, H. *Acta Crystalogr., Sect. B.* 46, 449, **1990**

18. Polosz , B.; Polosz W.; Gierlatka, S. *Acta Crystalogr., Sect. B.* 42, 653, **1986**

19. Dubrovskiĭ, G. B.; *Physics of the Solid State.* 40, 1557-1562, **1998**

20. Price, L. S.; Parkin, I.P.; Hardy, A. M. E.; Clark R. J. H. *Chem. Mater.* 11, 1792-1799, **1999**

21. Ibarz, A.; Ruiz, E.; Alvarez, S. *Chem. Mater.* 10, 3422-3428, **1998**

22. Brousse, T.; Lee, S. M.; Pasquereau, L.; Defives, D.; Schleich, D. M. *Solid State Ionics* 113-115, 51-56, **1998**

23. Bedard, R. L.;Vail, L. D.; Wilson, S. T.; Flanigen, E. M. *U.S. Patent.* 5,013,337. **1991**

24. Evans, J. S. O.; Price, S. J.; Wong, H. V.; O'Hare, D. *J. Am. Chem. Soc.* 120, 10837-10846, **1998**

25. Arora, S. K.; Patel, P. A.; Agarmal, M. K. *J. Mater. Sci. Lett.* 29, 3971, **1994**

26. Ettema, A. R. H. F.; de Groot, R. A.; Haas, C. *Phys. Rev. B.* 46, 7363, **1992**

27. Jiang, T.; Ozin, G. A.; Bedard, R. L. *Adv. Mater.* 6, 860-865, **1994**

28. Jiang, T.; Lough, A.J.; Ozin, G. A.; Bedard, R. L. *Chem. Mater.* 7, 245-248, **1995**

Chapter 3 – Search for the Tin Sulfide Tetramer

3.1 Introduction

Recent success with the use of the $Ge_4S_{10}^{4-}$ tetramer in the synthesis of dense[1], microporous[2] and mesoporous[3] germanium sulfides, and the complete absence of the tin counterpart of such syntheses makes the $Sn_4S_{10}^{4-}$ tetramer a likely candidate for study.

As mentioned previously there is one reference to this material in the literature, which stops at saying the material is 'completely characterized'. No details are given, nor is the molecule seen any further studies. Previous work in this group has synthesized this molecule and identified it through Reitveld refinement of powder x-ray diffraction (PXRD) data. Unfortunately the material proved insoluble and therefore could not readily be used as a precursor to other structures.

The original synthesis involved the reaction of SnS_2, tetramethyl ammonium hydroxide (TMAOH), thioacetamide and water in a 1:1:2:100 ratio. The base and the thioacetamide were dissolved in the water and added to the SnS_2 and the mixture brought to a boil while stirring. Over time, the solid turns a beige colour while the liquid over the solid develops a deep yellow hue. At this time the mixture is filtered hot, and the solid tetramer precipitated with the addition of ethyl acetate. Much of the solid reagent remains unreacted under these conditions.

3.2 $TMA_4Sn_4S_{10}$

To improve the yield more TMAOH was used – the base acts as a mineralizer for SnS_2. With two and a half equivalents of TMAOH per SnS_2, all of the solid reactants dissolve as the mixture is heated and stirred. However, attempts at precipitating out the tetramer from this solution, with ethyl acetate or other organic solvents, were entirely unsuccessful. Instead, PXRD analysis showed the solid thus recovered to be the $TMA_4Sn_2S_6$ dimer. The easiest way of making the germanium sulfide analogue is by a

hydrothermal reaction of stoichiometric amounts of the elements and TMAOH at 150 °C overnight. However this method also leads to the dimer when is adopted for use with tin.

Nevertheless this solution did prove to be somewhat fruitful: when left alone and open to air for about a month, dark golden crystals of cubic habit were recovered from the vessel that had held the solution. These beautiful crystals had to be separated from another set of crystals, which had also crystallized from the solution. The latter set of crystals was white, flat and spiky. Single crystal x-ray diffraction analysis showed that the white crystals were the dimer while the cubic crystals proved to be the tetramer (Figure 3.1, Tables 3.1-3.5).

3.3 ^{119}Sn NMR Studies

So, while this method was able to provide us with a new crystal structure, it obviously is completely useless as a synthetic route. To better understand what was happening, ^{119}Sn NMR spectroscopy was used. The most abundant NMR-active tin nucleus is ^{119}Sn, and it is present as roughly 10% of tin samples. This, combined with its somewhat high gyromagnetic ratio makes this a rather sensitive nucleus – nowhere near as easy as hydrogen to get a decent spectrum, but much more sensitive than ^{13}C. NMR is a very useful tool for studying tin compounds. In NMR the interaction of the target atom type (here, ^{119}Sn) with its chemical environment (i.e. the molecule that it is in) produces a unique magnetic environment, and hence a unique chemical shift for each chemical environment. So, different chemical shifts correspond to different structures.

Tin's chemical shift range is several thousand ppm in width, which allows different tin centres to be readily identified without fear of peaks overlapping. What is more important is that there is a unique band hundreds of ppm wide in which the resonances for a particular coordination number fall in. For four co-ordinate tin, this band is around zero ppm with respect to tetramethyl tin. Thus tin resonances within a few hundred ppm of zero are diagnostic of four coordinate tin.

Figure 3.2 shows a sequence of ^{119}Sn NMR spectra as a mixture of

$$2\ SnS_2 : 2\ CH_3CSNH_2 : 5\ TMAOH : 100\ H_2O$$

is heated to boiling. Early in the synthesis a single tin resonance is apparent, at around 73 ppm. As the reaction proceeds, a second resonance at around 54 ppm emerges and increases in intensity. This indicates tin is found in two different chemical structures. The

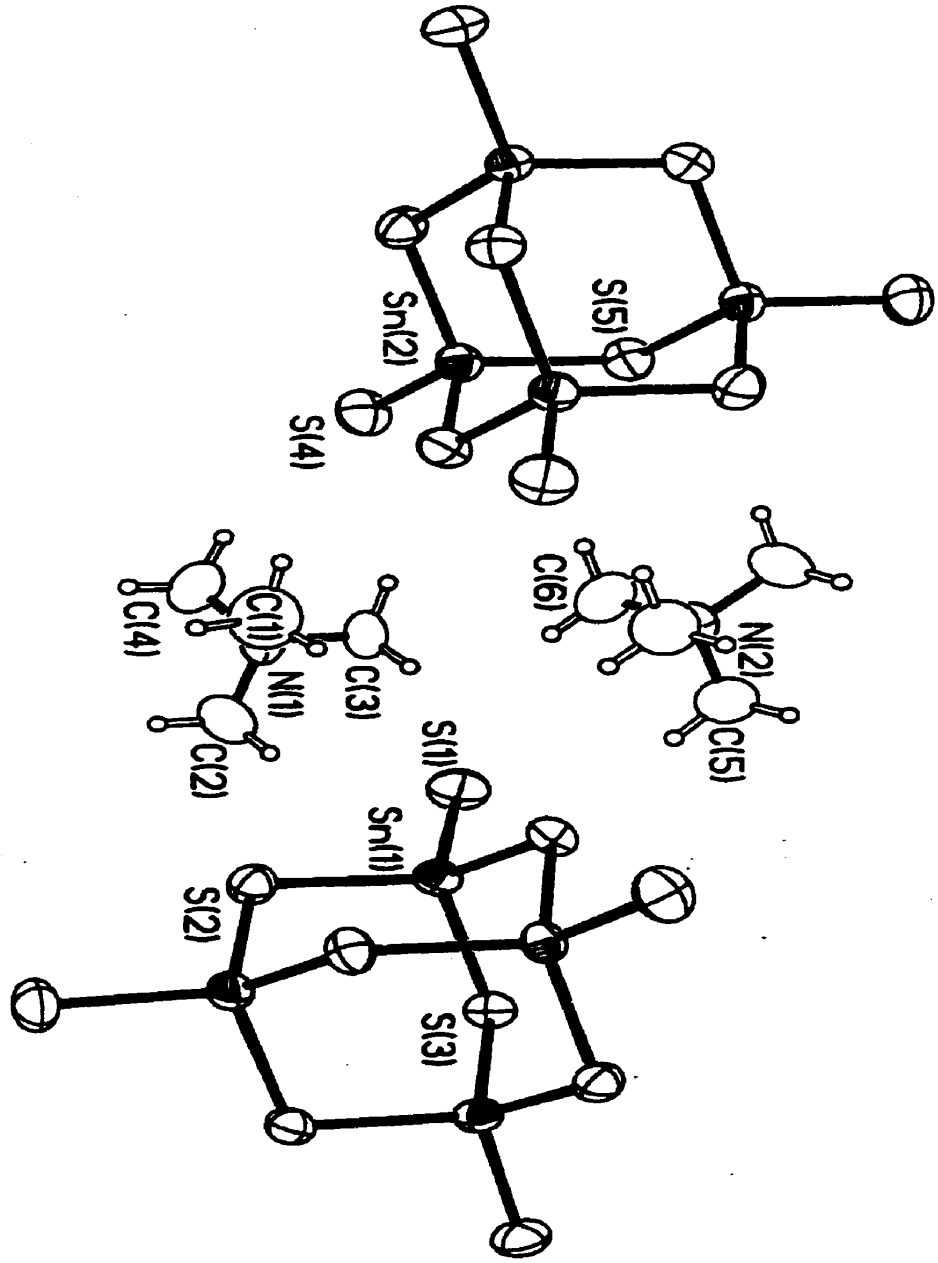

Figure 3.1: Crystal Structure of $TMA_4Sn_4S_{10}$. Diffraction data was collected Nonius-Kappa CCD equipped diffractometer. All data collection and refinement was performed by Dr. Alan Lough.

Table 3.1 Crystal data and structure refinement for Figure 3.1

Identification code	k9714
Empirical formula	$C_{16}H_{48}N_4S_{10}Sn_4$
Formula weight	1091.94
Temperature	293(2) K
Wavelength	0.71073 Å
Crystal system	Cubic
Space group	P-43n
Unit cell dimensions	a = 20.0220(10) Å alpha = 90° b = 20.0220(10) Å beta = 90° c = 20.0220(10) Å gamma = 90°
Volume, Z	8026.4(7) $Å^3$, 8
Density (calculated)	1.807 Mg/m^3
Absorption coefficient	2.995 mm^{-1}
F(000)	4256
Crystal size	0.18 x 0.18 x 0.20 mm
θ range for data collection	2.03 to 26.36°
Limiting indices	$0 \le h \le 25$, $0 \le k \le 25$, $0 \le l \le 25$
Reflections collected	8443
Independent reflections	1504 (R_{int} = 0.0475)
Refinement method	Full-matrix least-squares on F^2
Data / restraints / parameters	1504 / 0 / 111
Goodness-of-fit on F^2	0.758
Final R indices [$I>2\sigma(I)$]	R1 = 0.0197, wR2 = 0.0287
R indices (all data)	R1 = 0.0395, wR2 = 0.0303
Absolute structure parameter	-0.11(3)
Extinction coefficient	0.000076(11)
Largest diff. peak and hole	0.328 and -0.242 $eÅ^{-3}$

Table 3.2. Atomic coordinates [x 10^4] and equivalent isotropic displacement parameters [$Å^2$ x 10^3] for
U(eq) is defined as one third of the trace of the orthogonalized U_{ij} tensor.

	x	y	z	U(eq)
Sn(1)	5654(1)	1803(1)	736(1)	34(1)
Sn(2)	9303(1)	-697(1)	697(1)	38(1)
S(1)	6297(1)	1186(1)	1457(1)	54(1)
S(2)	5000	1101(1)	0	39(1)
S(3)	4919(1)	2504(1)	1391(1)	38(1)
S(4)	8644(1)	-1356(1)	1356(1)	59(1)
S(5)	10000	0	1396(1)	46(1)
N(1)	6617(2)	-813(3)	1515(2)	52(1)
N(2)	8348(2)	1652(2)	1652(2)	45(2)
C(1)	6803(4)	-588(3)	830(3)	84(2)
C(2)	5905(3)	-659(3)	1650(3)	67(2)
C(3)	7043(3)	-447(3)	2016(3)	59(1)
C(4)	6749(4)	-1550(3)	1579(4)	75(2)
C(5)	7923(3)	2077(3)	2077(3)	67(3)
C(6)	8218(4)	934(3)	1814(3)	73(2)

chemical shifts, being so close to zero ppm, show that in both molecules tin is coordinated by four atoms.

A T_1 study of these two resonances showed that they both have T_1 decay times of around 13 ms. NMR spectroscopy, as practiced here, works by broadband excitation followed by observing the decay of the excited states. The T_1 time is a measure of how quickly this relaxation occurs. The experimental conditions used here ensure that tin centres in both chemical environments have sufficient time to relax to thermal equilibrium before they are re-excited. So, when we look at a certain peak, we are looking at tin in a particular chemical environment. And when we look at the area under that peak, we are looking at the population of that chemical environment. For example, under these conditions a 1:2 ratio in peak areas means that there is twice as much tin in one chemical environment compared to the other.

Table 3. Bond lengths [Å] and angles [°] for

Sn(1)-S(1)	2.295(2)	Sn(1)-S(3)#1	2.4125(13)
Sn(1)-S(3)	2.4206(13)	Sn(1)-S(2)	2.4215(11)
Sn(2)-S(4)	2.285(4)	Sn(2)-S(5)	2.4199(12)
Sn(2)-S(5)#2	2.4199(12)	Sn(2)-S(5)#3	2.4199(12)
S(2)-Sn(1)#4	2.4215(11)	S(3)-Sn(1)#5	2.4125(13)
S(5)-Sn(2)#6	2.4199(12)	N(1)-C(2)	1.484(7)
N(1)-C(1)	1.490(7)	N(1)-C(4)	1.504(8)
N(1)-C(3)	1.508(6)	N(2)-C(5)	1.472(13)
N(2)-C(6)#7	1.497(7)	N(2)-C(6)#3	1.497(7)
N(2)-C(6)	1.497(7)		

S(1)-Sn(1)-S(3)#1	107.99(5)	S(1)-Sn(1)-S(3)	108.21(5)
S(3)#1-Sn(1)-S(3)	109.43(3)	S(1)-Sn(1)-S(2)	111.96(5)
S(3)#1-Sn(1)-S(2)	109.53(4)	S(3)-Sn(1)-S(2)	109.67(4)
S(4)-Sn(2)-S(5)	109.38(4)	S(4)-Sn(2)-S(5)#2	109.38(4)
S(5)-Sn(2)-S(5)#2	109.56(4)	S(4)-Sn(2)-S(5)#3	109.38(4)
S(5)-Sn(2)-S(5)#3	109.56(4)	S(5)#2-Sn(2)-S(5)#3	109.56(4)
Sn(1)-S(2)-Sn(1)#4	109.05(7)	Sn(1)#5-S(3)-Sn(1)	109.46(5)
Sn(2)-S(5)-Sn(2)#6	109.29(8)	C(2)-N(1)-C(1)	110.2(6)
C(2)-N(1)-C(4)	110.9(5)	C(1)-N(1)-C(4)	109.4(5)
C(2)-N(1)-C(3)	108.8(4)	C(1)-N(1)-C(3)	108.8(4)
C(4)-N(1)-C(3)	108.7(5)	C(5)-N(2)-C(6)#7	109.3(4)
C(5)-N(2)-C(6)#3	109.3(4)	C(6)#7-N(2)-C(6)#3	109.7(4)
C(5)-N(2)-C(6)	109.3(4)	C(6)#7-N(2)-C(6)	109.7(4)
C(6)#3-N(2)-C(6)	109.7(4)		

Symmetry transformations used to generate equivalent atoms:

#1 z+1/2,-y+1/2,-x+1/2 #2 y+1,-z,-x+1 #3 -z+1,-x+1,y

#4 -x+1,y,-z #5 -z+1/2,-y+1/2,x-1/2 #6 -x+2,-y,z

#7 -y+1,z,-x+1

The peak at 54 ppm has been previously assigned to the $Sn_2S_6^{4-}$ dimer[4]. Note that although there are two tin centres in this molecule, the molecule's symmetry puts them both in an identical magnetic environment – hence a single resonance for this molecule. So, one-half the area under this peak is proportional to the amount of dimer present. However, vibrational disorder and symmetry breaking by distorting the chemical environment can account for the broader shape of the dimer peak. As for the second resonance, it was confirmed to be the SnS_4^{4-} monomer by repeating Krebs' synthesis[5] for the monomer and looking at its NMR spectrum (Figure 3.3). Since there is only one tin atom per molecule, the area under this curve is proportional to the amount of monomer present. It should be noted that this reaction ($Na_2S + SnCl_4$) has also been used by Krebs[6] to make the dimer by adjusting the reactant ratios. So it is not surprising to also see the

Table 3.4. Anisotropic displacement parameters ($Å^2 \times 10^3$) for Figure 3.1. The anisotropic displacement factor exponent takes the form: $-2\pi^2 [(ha^*)^2 U_{11} + ... + 2hka^* b^* U_{12}]$

	U11	U22	U33	U23	U13	U12
Sn(1)	32(1)	36(1)	33(1)	4(1)	-2(1)	2(1)
Sn(2)	38(1)	38(1)	38(1)	3(1)	3(1)	-3(1)
S(1)	54(1)	55(1)	52(1)	14(1)	-10(1)	13(1)
S(2)	43(1)	34(1)	41(1)	0	-2(1)	0
S(3)	39(1)	45(1)	31(1)	2(1)	0(1)	8(1)
S(4)	59(1)	59(1)	59(1)	11(1)	11(1)	-11(1)
S(5)	49(1)	53(1)	37(1)	0	0	-5(1)
N(1)	61(4)	51(3)	45(3)	-6(3)	-5(2)	-15(3)
N(2)	45(2)	45(2)	45(2)	5(2)	-5(2)	-5(2)
C(1)	105(6)	107(6)	40(4)	5(4)	3(4)	-11(5)
C(2)	52(4)	80(4)	67(5)	4(4)	-5(3)	-13(4)
C(3)	60(4)	54(4)	62(4)	-10(3)	-13(3)	-12(3)
C(4)	91(6)	42(4)	92(5)	-8(4)	5(4)	-7(4)
C(5)	67(3)	67(3)	67(3)	-4(4)	4(4)	4(4)
C(6)	87(5)	48(4)	85(5)	-2(4)	2(5)	4(4)

Table 3.5. Hydrogen coordinates (x 10^4) and isotropic displacement parameters ($Å^2 \times 10^3$) for Figure 3.1

	x	y	z	U(eq)
H(1A)	6780(23)	-110(4)	808(7)	126
H(1B)	6499(15)	-778(20)	512(3)	126
H(1C)	7249(10)	-731(21)	731(10)	126
H(2B)	5828(5)	-190(4)	1588(19)	100
H(2C)	5798(6)	-781(18)	2102(7)	100
H(2D)	5628(3)	-908(15)	1348(13)	100
H(3A)	6978(15)	26(3)	1966(13)	88
H(3B)	7505(3)	-553(15)	1942(12)	88
H(3C)	6918(13)	-579(14)	2460(3)	88
H(4A)	6509(17)	-1786(3)	1238(14)	112
H(4B)	6604(21)	-1701(5)	2011(9)	112
H(4C)	7219(4)	-1633(4)	1530(22)	112
H(5A)	7993(38)	1963(3)	2537(35)	101
H(5B)	7463(4)	2007(35)	1963(38)	101
H(5C)	8037(35)	2537(38)	2007(3)	101
H(6A)	8315(18)	854(5)	2277(6)	110
H(6B)	8498(14)	656(3)	1541(14)	110
H(6C)	7758(6)	832(6)	1728(18)	110

dimer produced, but in a much smaller amount. It is interesting that apart from the most intense (monomer) peak, and the second most intense (dimer) peak, there are two other tin resonances.

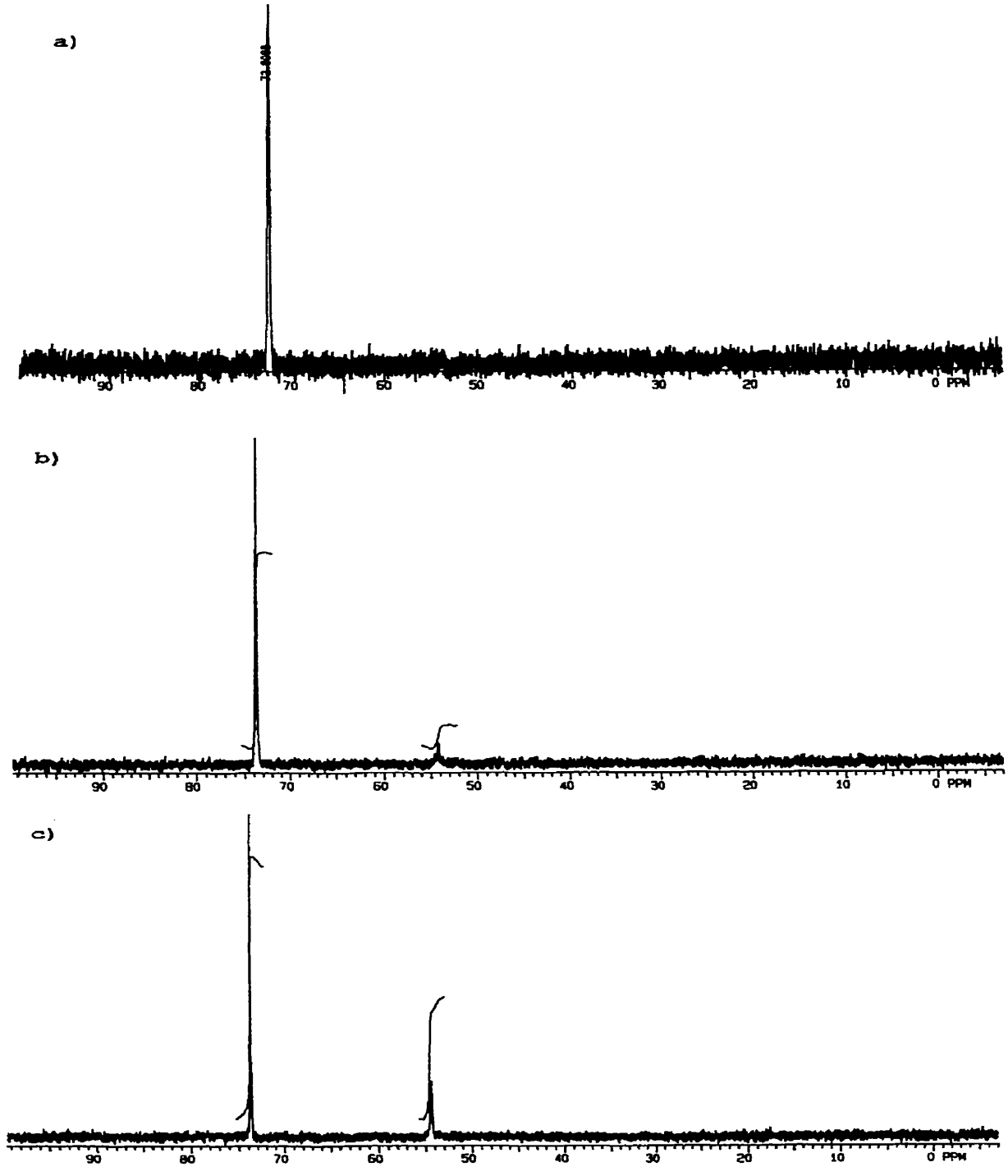

Figure 3.2: ^{119}Sn liquid NMR spectra of the mixture $2SnS_2$:$2CH_3CSNH_2$:5TMAOH:$100H_2O$ as it is heated.(continued)

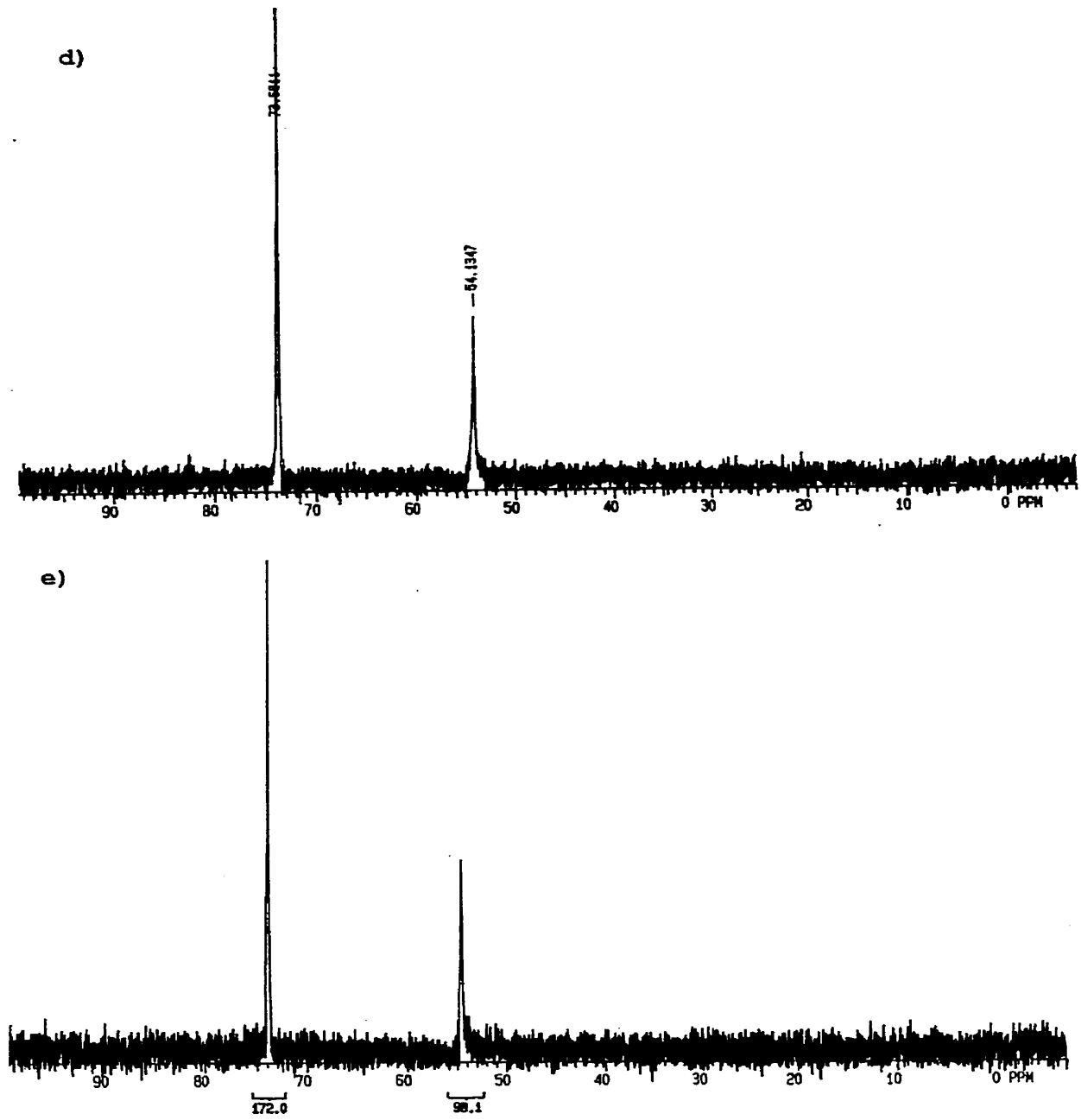

Figure 3.2:(continued) a) 40 °C, b) 55 °C, c) 70 °C, d) 80 °C, e) 84 °C. The sequence represents a total reaction time of one hour. All spectra were recorded on a Varian Gemini spectrometer with a ^{1}H Larmor frequency of 300 MHz. Tetramethyl tin is the standard, referenced at 0 ppm. All solutions contain D_2O for lock signal.

These two resonances at 58 and 67 ppm were occasionally seen throughout this study, but remain unassigned to any particular molecule.

With the NMR data at hand we can try to understand what happens during this reaction. Under these reaction conditions thioacetamide undergoes hydrolysis to give H_2S, which is a source of S^{2-} anions:

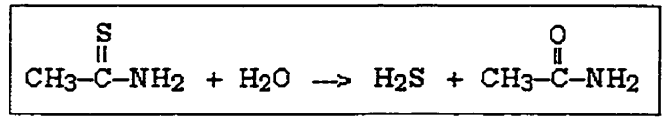

Recall that tin in SnS_2 is six coordinate. As it is mineralized – that is removed from the dense solid state structure – the coordination number must decrease, since there are only two sulfurs for each tin. Only by sharing sulfur atoms in the dense structure can the coordination number reach six. It has been previously mentioned that all molecular tin sulfides are four coordinate. The easiest way for tin atoms to accommodate this coordination number in this environment is to bond with two additional sulfide ions, to go from SnS_2 to SnS_4^{4-}. Note that tin remains in the +4 oxidation state throughout.

The breakdown of thioacetamide produces H_2S, which releases H^+ cations as it delivers sulfide anions. Thus, we expect the solution to acidify as the reaction proceeds. This suggests that the conversion of the monomer to the dimer proceeds through an acid mediated condensation.

It is interesting that a solution containing tin sulfide monomer and dimer molecules can lead to the tetramer (Figure 3.1) when left open to air.

Given the reasoning above about the conversion of the monomer to the dimer, it should be possible to alter the final synthetic mixture by adjusting the pH. Figures 3.4 and 3.5 contain NMR spectra for syntheses in all ways identical with the one above, except for the use of four and six equivalents TMAOH. It can be seen that with more base present the monomer yield is nearly 100% (Figure 3.5). Although the use of less base fails to produce an all dimer solution, the solution corresponding to Figure 3.4 is definitely enriched in dimer with respect to Figure 3.2e.

What is more interesting is that the dimer to monomer transition, or its reverse can be affected post-synthesis with the appropriate addition of base or acid. In Figure 3.6 is a sequence of NMR spectra. Starting with the original all dimer solution, subsequent spectra correspond to portions of the original solution to which different amounts of a

NaOH solution have been added. Similarly Figure 3.7 chronicles the transformation of the monomer into the dimer with the addition of strong acid (acetic or nitric). It is important to note the total conversion of one species to the other.

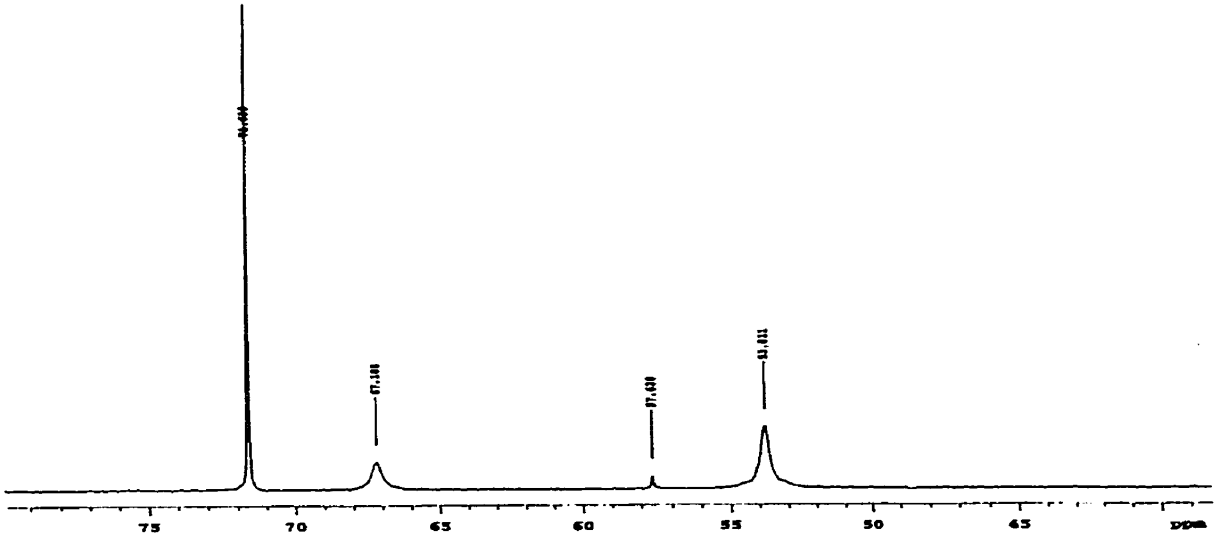

Figure 3.3: ^{119}Sn liquid NMR spectrum of a solution obtained by the addition of $SnCl_4$ to Na_2S dissolved in water. The tin:sulfur ratio is 1:4. The peak at 53.811 ppm is previously identified as belonging to the $Sn_2S_6^{4-}$ dimer. As the above solution was used to make the SnS_4^{4-} molecule, the large peak at 71.639 ppm is assigned to this molecule. The identities of the remaining resonances are not known.

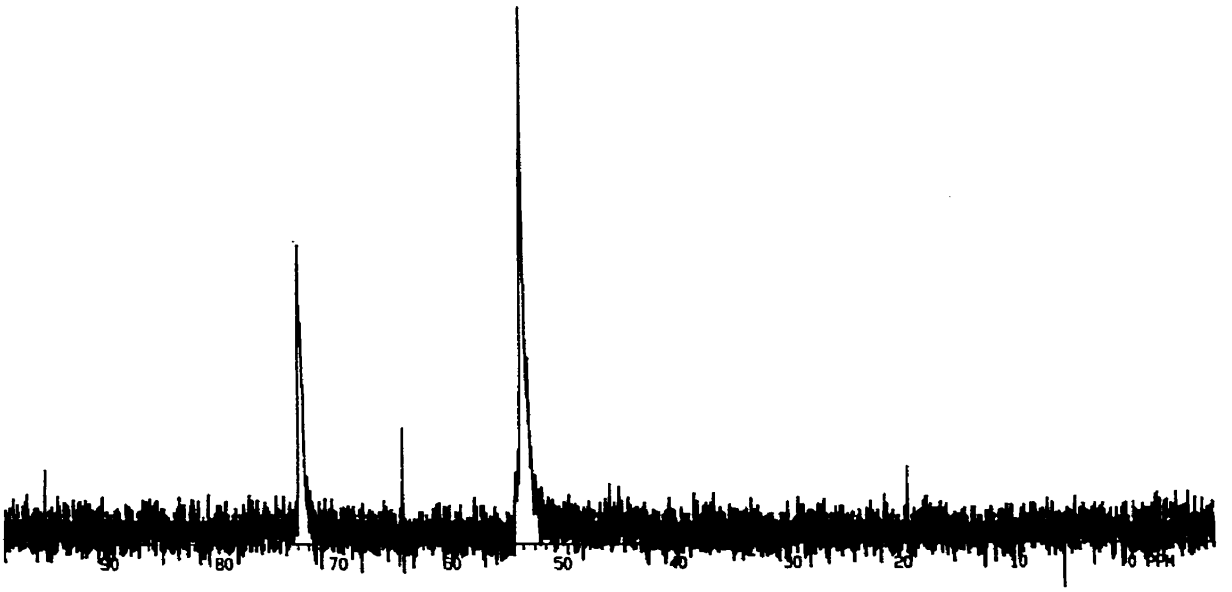

Figure 3.4: ^{119}Sn liquid NMR spectrum of the mixture $2SnS_2$:$2CH_3CSNH_2$:4TMAOH:$100H_2O$ after it has been heated to boiling. Presence of less base increases the amount of dimer produced.

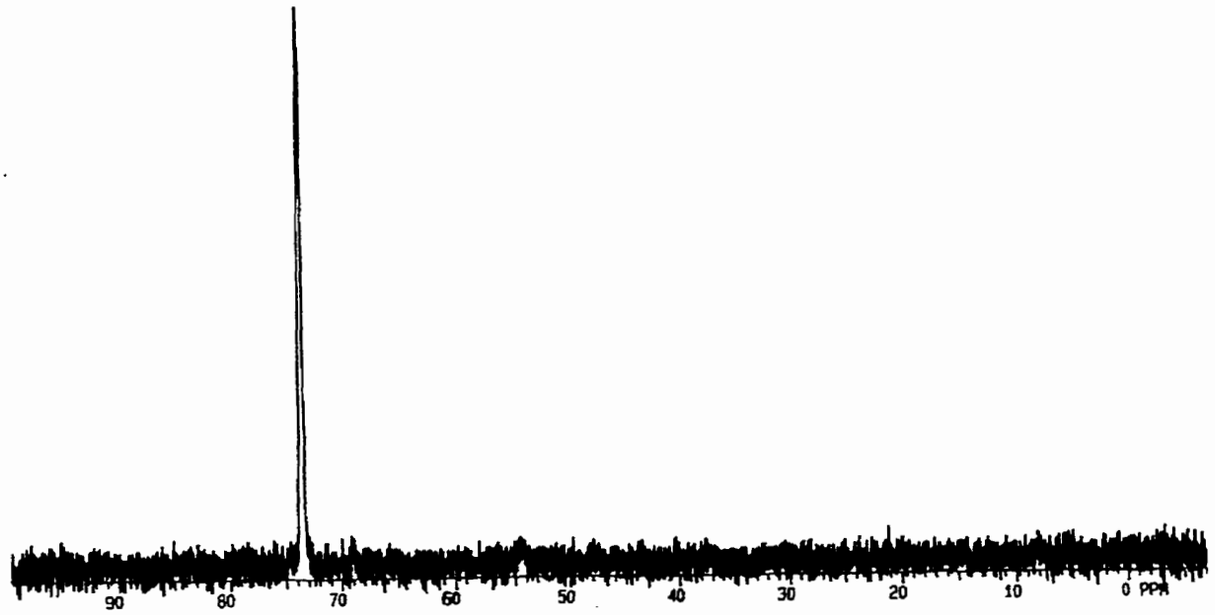

Figure 3.5: ^{119}Sn liquid NMR spectrum of the mixture $2SnS_2$:$2CH_3CSNH_2$:6TMAOH:100H_2O after it has been heated to boiling. With this amount of base present dimer production is entirely suppressed.

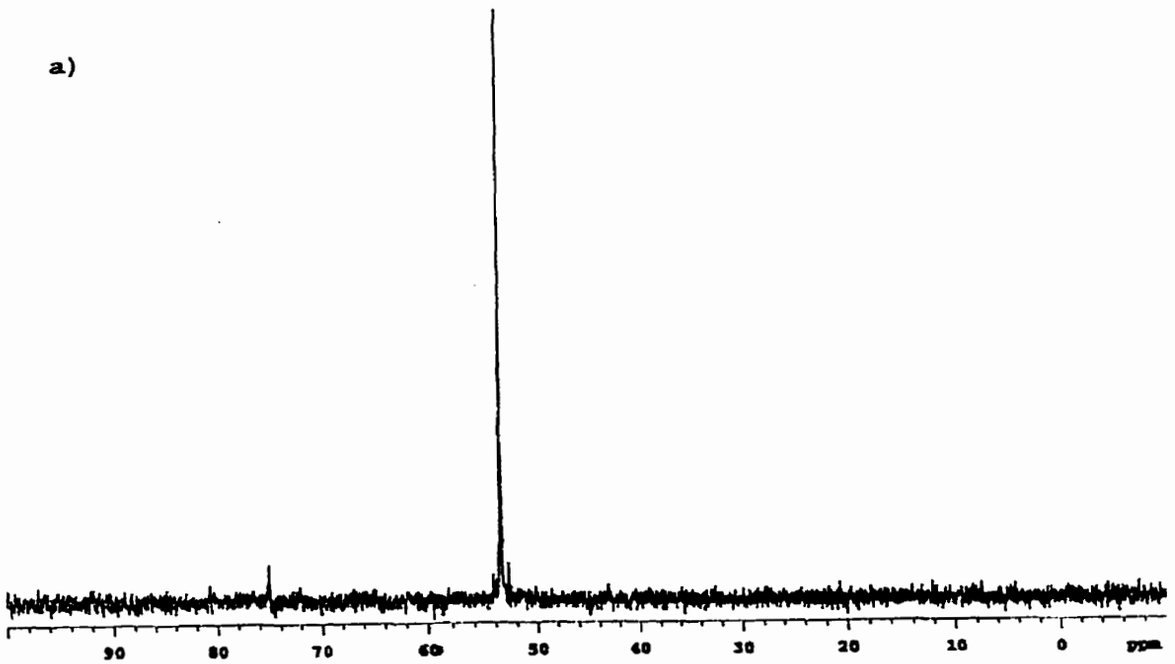

Figure 3.6a: ^{119}Sn liquid NMR spectra showing the conversion of dimer into monomer as KOH solution is added. pH 10.8 (continued)

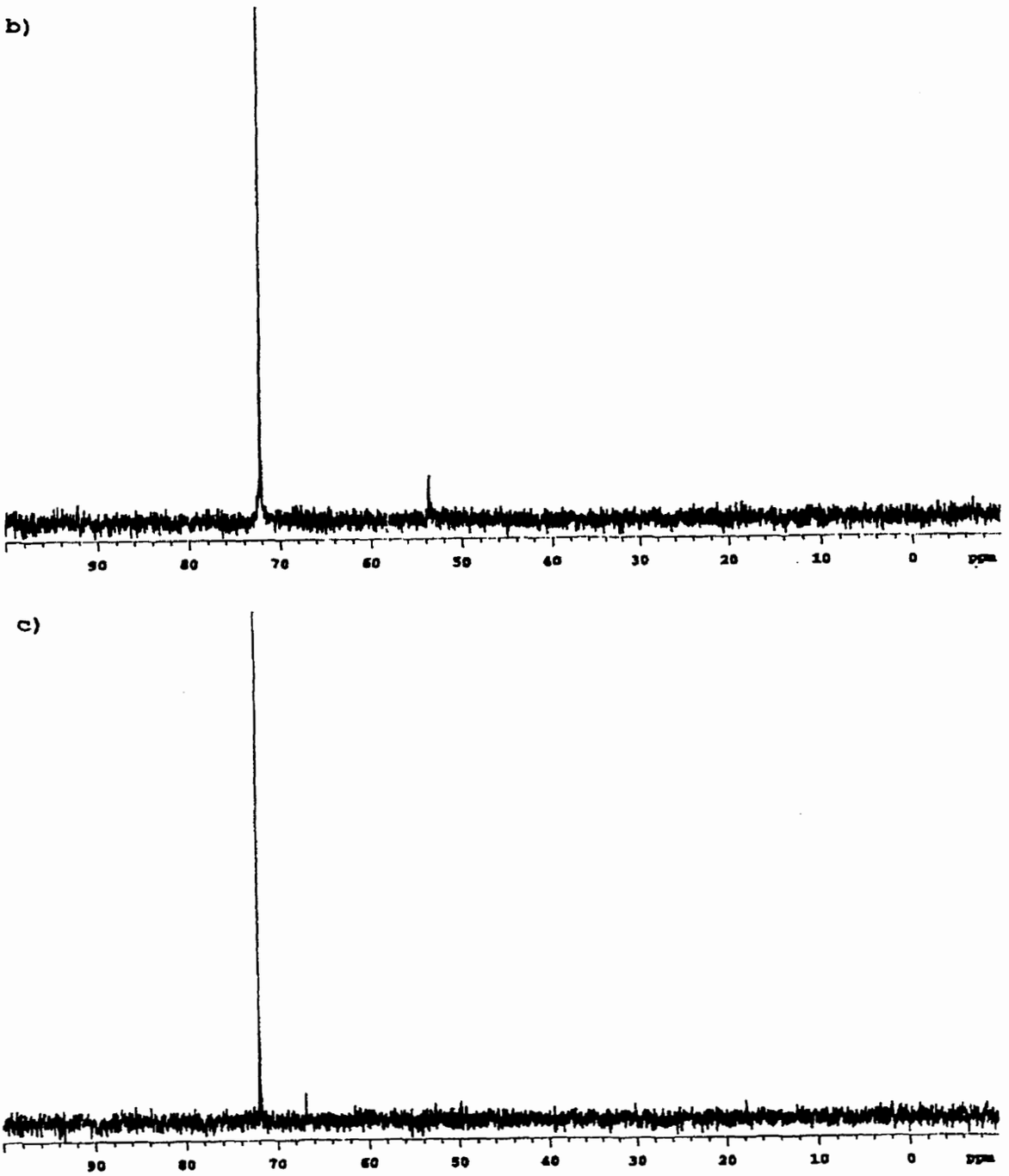

Figure 3.6 (continued) b) pH 13.6, c) pH 14.6

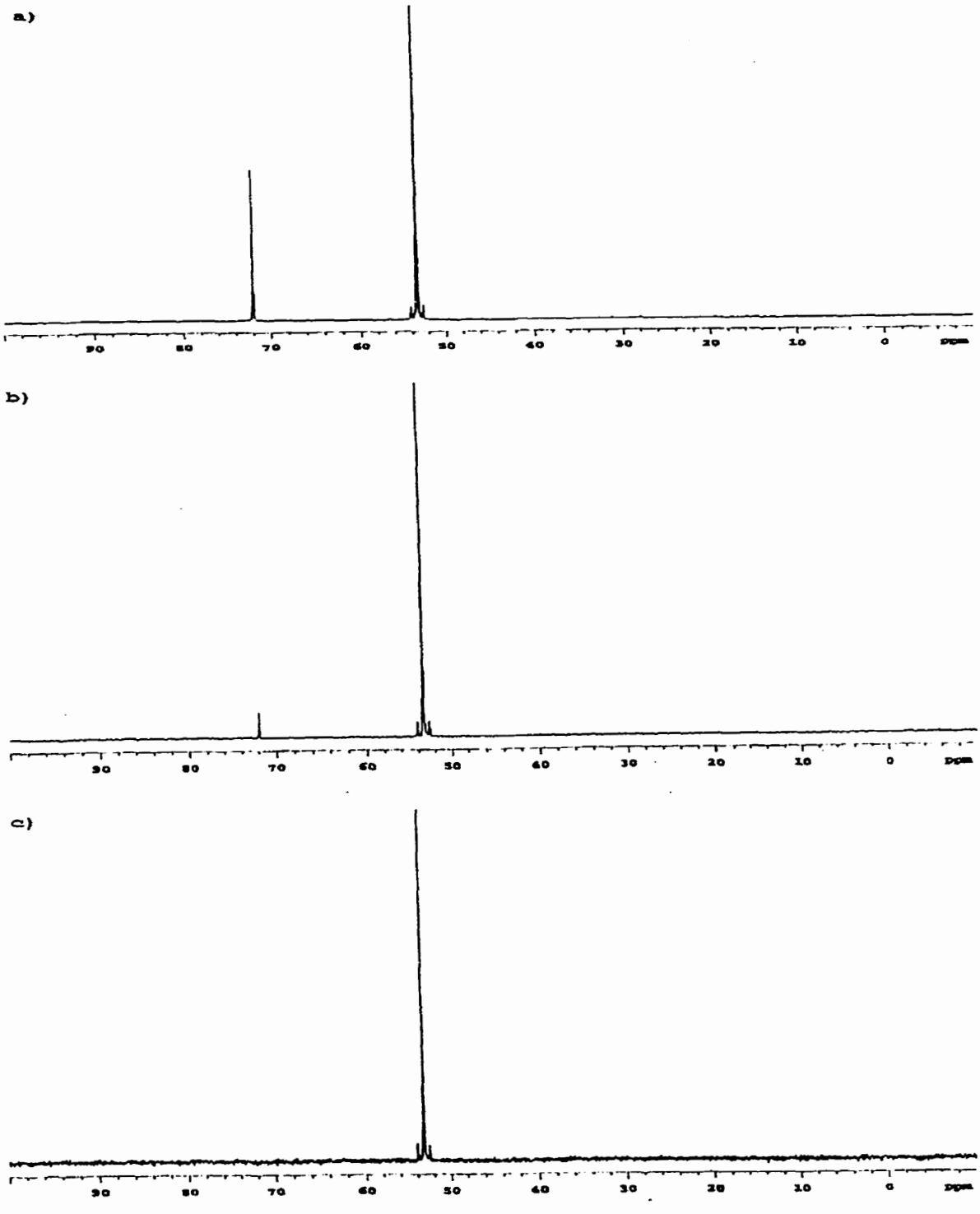

Figure 3.7: ^{119}Sn liquid NMR spectra showing the conversion of monomer into dimer as HCl solution is added. a) pH 12.2, b) pH 11.3, c) pH 10.1

An obvious question is whether further condensation can produce the tetramer. Unfortunately, as more acid is added and the pH of these solutions dips below 7 an amorphous (by PXRD) yellow-white solid forms. It is known that slow acidification of a $TMA_4Sn_2S_6$ solution (by bubbling CO_2 through the solution) leads to the formation of the SnS-1 structure[4]. The condensation to the tetramer using this method may be possible with the use of a much bulkier counter cation. That is to say, if the counter ion is so big that assembly into sheets is impossible, condensation may proceed to the tetramer.

3.4 References

1. MacLachlan, M. J.; Petrov, S.; Bedard, R. L.; Manners, I.; Ozin, G. A. *Angew. Chem. Int. Ed. Engl.* 37, 2076-2079, **1998**

2. Bowes, C. L.; Huynh, W. U.; Kirkby, S. J.; Malek, A.; Ozin, G. A.; Petrov, S.; Twardoski, M.; Young, D.; Bedard, R. L., Broach, R. *Chem. Mater.* 8, 2147-2152, **1996**

3. MacLachlan, M. J.; Coombs, N.; Bedard, R. L.; White, S.; Thompson, L. K.; Ozin, G. A. *J. Am. Chem. Soc.* 121, 12005-12017, **1999**

4. Jiang, T. *Porous Tin (IV) Sulfide Materials*. Ph. D. Thesis, University of Toronto. **1998**

5. Schiwy, W.; Pohl, S.; Krebs, B. *Z. Anorg. Allg. Chem.* 402, 77-86, **1973**

6. Krebs, B.; Pohl, S.; Schiwy, W. *Z. Anorg. Allg. Chem.* 393, 241-252, **1972**

Chapter 4 – New Meso Tin Sulfides

4.1 Introduction

As mentioned in Chapter 2, these new materials have very interesting characteristics. Their properties are governed by the fact that they are organic/inorganic hybrids. This structure gives the chemist an opportunity to tune the nature of the material.

The original materials used hexadecylamine (HDA) as the organic template and counter cation. A reaction mixture of 2.6 HDA : 2 $(NH_4)_2S$: $SnCl_4$: 16 NH_4OH : 260 H_2O was brought together in an Enflon reaction vessel sealed in a stainless steel bomb and reacted at 150 °C for 19 hours. Elemental analysis showed the material to have an empirical formula of $Sn_{1.00}S_{2.07}HDA_{2.34}H_2O_{2.23}$. The most interesting about this analysis is that the tin to sulfur ratio is 1.00:2.07, which among the lamellar tin sulfides is the closest to that of SnS_2. As SnS_2 is neutral, any excess sulfur in the structure indicates excess negative charge which must be counter balanced by the organic cation. In the case of meso tin, the tin to sulfur ratio indicates that the majority of the HDA will be neutral.

The most interesting property of meso tin is its mesogenic character, as indicated by thermal analysis, variable temperature PXRD and polarized optical microscopy. PXRD on heating first shows the loss of order associated with the layer structure of the organic template, and then as temperature is increased the loss of order associated with the tin sulfide. Differential scanning calorimetry (DSC) sees these two order-disorder transitions as two distinct endothermic events. Similarly, upon cooling two exothermic events are seen as the order is re-established.

4.2 Meso Tin Sulfides with Different Templates

It turns out that HDA is only one suitable template for synthesizing meso tin sulfides. For tetradecylamine (TDA) as the template, a mixture of 2.5 TDA : 6 $(NH_4)_2S$: $SnCl_4$: 16 NH_4OH : 450 H_2O, tumbled overnight in a 150 °C oven produced a highly ordered material. In Figure 4.1 a typical PXRD pattern for TDA-meso tin can be seen. It is reasonably well ordered, with five orders of diffraction visible. The layering of the

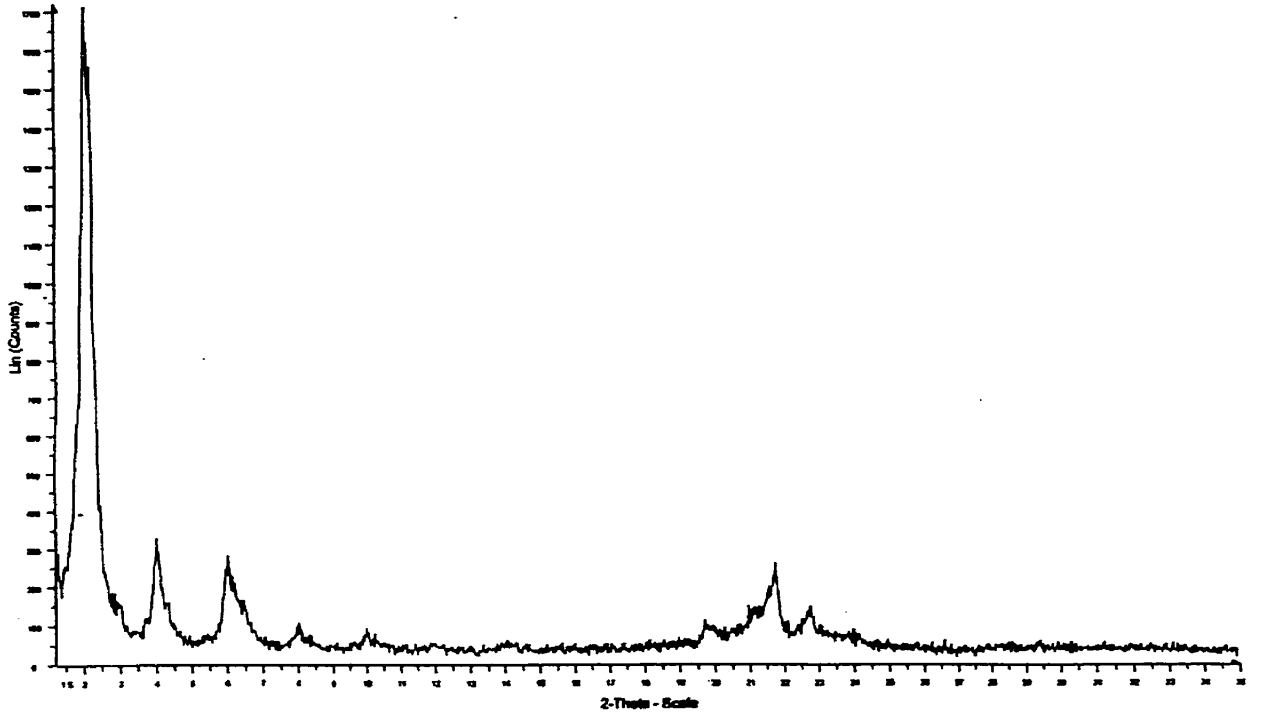

4.1: PXRD pattern of TDA-meso tin sulfide. Five orders of lamellar reflection are readily visible, down to roughly 10° 2θ. The 100 reflection corresponds to an layer spacing of 46 Å. Features between 20° and 24° 2θ correspond to order within the tin sulfide sheet. All PXRD data were collected on a Siemen's D5000 diffractometer with equipped with a Kevex solid state detector.

material is clearly seen in the TEM image in Figure 4.2. It should be noted that a TEM of the surfactant alone would not have enough contrast between its layers to produce image similar to that seen in Figure 4.2. It is the presence of tin with its many electrons that provides this contrast.

The interlayer spacing for TDA-meso tin sulfide of 45 Å compares well to that of 51 Å for the HDA templated material. Note that the interlayer spacing corresponds to the distance between successive tin sulfide planes, which are separated by two layers of the template. On going from HDA to TDA a total of four carbons are lost. Four times 1.25 Å, which is the length of a fully extended alkane chain is precisely equal to the difference in the interlayer spacing between the two materials.

Evidence of mesogenic character for TDA-meso tin sulfide can be seen in Figure 4.3. Here are seen two DSC traces. One is of the original HDA templated material and the other of the newer TDA templated. The shapes of the two curves are very similar, with the newer material showing broader first transition but a narrower second transition.

Figure 4.2: A TEM image of a TDA-meso tin sulfide. Magnification 345 000 times. Obtained by Dr. Neil Coombs.

As expected the first order-disorder transtion of the TDA templated material happens at a lower temperature. Recall that this transition is the loss of order in the organic layer. We expect that shorter alkane chains interact more weakly with each other and require less thermal energy to lose their ordered structure. What is more interesting is that the second transition – the loss of order in the tin sulfide sheet – also happens at a lower temperature. This is either a synergy effect in this hybrid material, or indicates different tin sulfide structures.

It has also been possible to produce meso tin sulfides with long chain amine templates, with the chain lengths of eight, 12 and 13 carbons. Figure 4.4 shows how the interlayer spacing varies with the template chain length. Note that the syntheses with templates other than HDA and TDA have not been optimized, so the Figure can only illustrate the trend. Nevertheless the trend is rather reassuring.

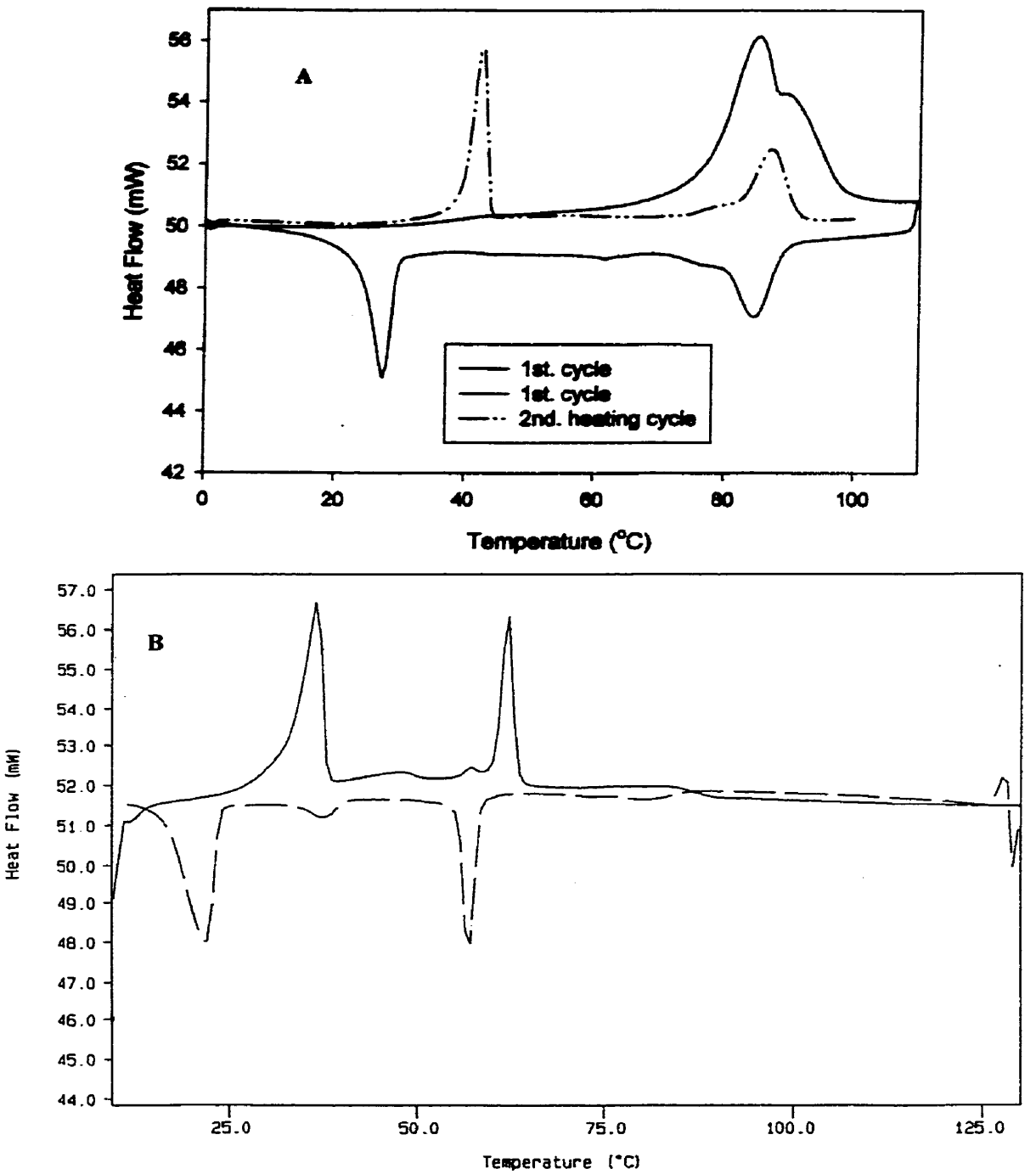

Figure 4.3: DSC traces of a) HDA[1]- and b) TDA-meso tin sulfides. The material with the shorter organic surfactant undergoes order-disorder transitions at lower temperatures.

Of all these materials perhaps the most interesting is the one templated with octylamine. Unlike the other amines which are solids at room temperature, octylamine is

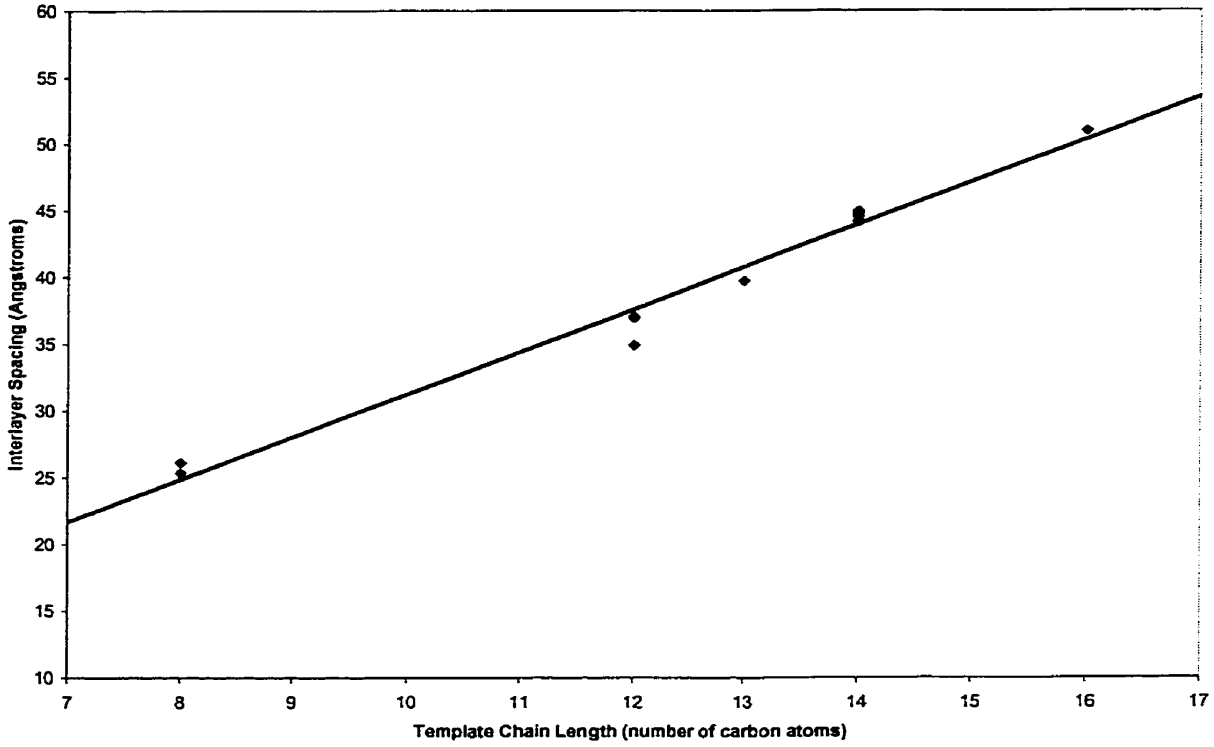

Figure 4.4: Variation in layer spacing for various meso tin sulfides as measured by PXRD. There is in general a good fit to a straight line.

a liquid. However the final product is a solid like the rest of the series, highlighting the importance of the organic/inorganic interaction in this class of materials.

4.3 References

1. Jiang, T. *Porous Tin (IV) Sulfide Materials*. Ph. D. Thesis, University of Toronto. **1998**

Chapter 5 – An EXAFS Study of Meso Tin Sulfides

5.1 Introduction

EXAFS (Extended X-ray Adsorption Fine Structure) spectroscopy is a photoelectron spectroscopy in which x-rays photoionize a K- or L- shell core electron. Since the energies of these electronic levels are unique to each atom, the technique is atom specific. This has the great advantage of preventing interference from different atoms, and the technique is useful even if the target atom is present in very low concentrations. For this reason EXAFS is often used in analysis of catalysts.

EXAFS provides information about local structure around each atom of the target type. In this regard it differs from other techniques, such as x-ray diffraction, which provide information on relatively long range order. Since it not a diffraction technique it can be used with disordered systems such as glasses, amorphous materials and even liquids.

Because of the need to record an absorption spectrum the technique requires a bright and tunable x-ray source. The commissioning of synchrotron radiation facilities has led to great advances in the number of researchers using this technique, which has spurred on the creation of theoretical treatments of increasing complexity.

5.2 Synchrotron radiation[1]

Synchrotron radiation was at first a nuisance at particle accelerators, which were built to study the composition of elementary particles by first accelerating and then smashing them. These moving charged particles can be accelerated by magnetic fields. As is familiar from more conventional X-ray methods, accelerating charges give off electromagnetic radiation. From a conventional x-ray tube this is called the Bremsstrahlung (breaking) radiation. Most particle accelerators increase the energies of the particles by accelerating them around a circular vacuum tube. To this kind of research

synchrotron radiation is a nuisance since it leads to loss of particle energy as light is radiated away.

The bane of one researcher is the boon of another. It was soon realized that this phenomenon could provide light of exceptional brilliance at wavelengths normally unavailable to scientists. Brilliance is a term often encountered in the synchrotron literature, referring both to the brightness (photon/s) and to the collimation of a beam of light. The first synchrotron radiation beam lines were set up in a parasitic mode at existing particle accelerators. To this day jargon lingers from these humble beginnings. The original experimental end stations were crowded in between existing equipment, and thus were tiny and cramped. So they were called hutches, and still are, even though the end stations at newer facilities are full sized rooms.

From these humble, parasitic, first generation light sources have evolved today's dedicated third generation synchrotrons. Along the way the most significant advance has been the development of the insertion devices that marked the arrival of the third generation machines. The second generation facilities are purpose built light sources; they lack insertion devices, and are modest in diameter in comparison with today's top facilities.

Synchrotron radiation was first seen as charged particles were bent into their circular tracks. Thus the simplest way of getting light out of a synchrotron is from the bending magnets. This is kind of a 'free' radiation: A workable synchrotron has to be circular (so that it can be loaded with charged particles and a current maintained), and a circular accelerator needs bending magnets to keep the charge in the beam tube.

Insertion devices are a whole different game from bending magnets. Their sole purpose is to produce brilliant light. There are two kinds – undulators and wigglers – and both consists of banks of permanent magnets that fit over the particle beam in the straight sections of the accelerator between the bending magnets. Wigglers have high field magnets that are relatively far apart while undulators are made up of lower field magnets much more closely placed. Wigglers produce less brightness but provide a wider spectrum of light. The output from undulators is very spiky, but is still tunable over a

range of wavelengths. This tuning, however, requires actually modifying the insertion device.

So today's third generation synchrotrons can be very large (over a kilometre in circumference) and they possess three different ways of producing light– bending magnets, wigglers and undulators. Making the facility large, and the use of superconducting bending magnets allow for very high particle energies. These advances have provided unprecedented brilliance for hard x-rays.

Another advantage of a large accelerator is that it provides lots of room around its circumference for experimental end stations. This is a good thing as use of these facilities is continually on the rise, especially for the biomedical and materials sciences. This has led to proposed construction of many new facilities. Most of these are much smaller than the initial third generation machines and are comparable with the second generation facilities in size. The main reason for this downsizing is to keep costs down. However these new facilities, such as the Canadian Light Source under construction at the University of Saskatchewan, make full use of insertion devices to provide useful light of diverse energies and brilliances. It should also be noted that most second-generation facilities are also undergoing refits. These modifications include incorporation of insertion devices and use of superconducting bending magnets, which allows higher energy beams.

Fourth generation facilities being dreamt of are a radical departure from today's machines. Designed around linear accelerators, these new machines will produce their light from free electron lasers, providing orders of magnitude increases in brilliance. These machines will not replace today's facilities. Today's machines are ideally suited to current needs, especially for the biological sciences and for what are now routine analyses like EXAFS. The fourth generation devices will open up brand new avenues of research such as x-ray microscopy and holography and also expanding the availability of real time studies.

5.3 X-ray Absorption Phenomena

When an x-ray photon impinges on an atom one of two things can happen. Either the photon is too low in energy to ionize the atom, or it is not. If the energy is high enough the photon is absorbed and the atom loses a photoelectron. Thus, to a rough approximation, if we look at the x-ray absorption spectrum of an atom around the binding energy of its 1s (K-shell) electrons, we should see a step: At low energy, the photons are not energetic enough to photoionize the atom and the absorbance is low. Just below the binding energy the absorbance jumps up as photons are absorbed to excite electrons into unoccupied orbitals. Past the binding energy absorption leads to photoionization.

This, then, is the most important step in EXAFS spectroscopy: The production of the photoelectron. Of course, if things were as simple as sketched above, there would be no hope of garnering any information other than the binding energy of the core electron. So we must look into this phenomenon with greater detail.

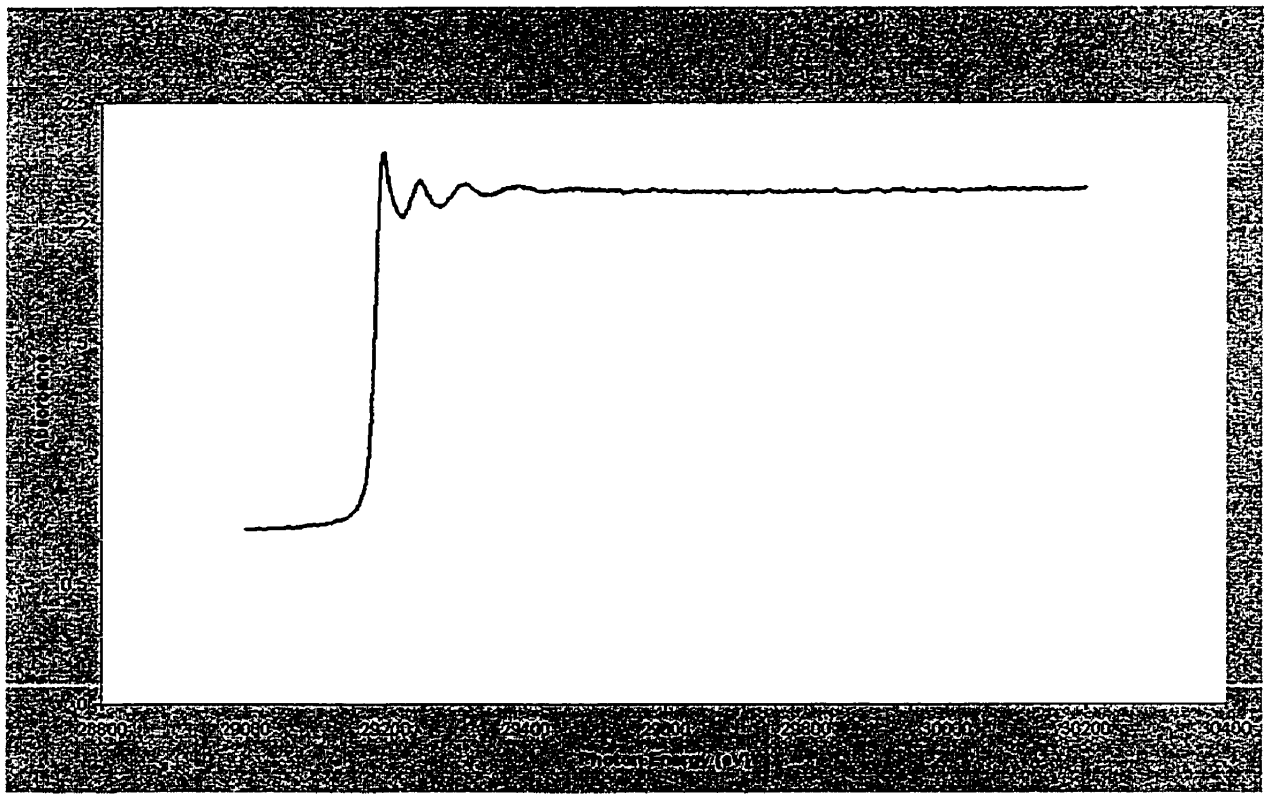

Figure 5.1: X-ray absorption spectrum of a TDA-meso tin sulfide.

In Figure 5.1 a real x-ray absorption spectrum of a meso tin sulfide is shown. The overall outline of a step is present but so are other details. Typically such a spectrum is divided into three sections, each of which can provide information about the sample. The location of the absorption is called the absorption edge, or simply the edge. In theory the edge is located at precisely the photon energy required for photoionization. The region at lower energies than the edge, but still above the background is called the pre-edge. This region corresponds to photoexcitation from the core to excited states of the target atom.

From the edge to about 30 eV above it is the region called the near edge. This region is referred to as the NEXAFS (Near Edge X-ray Absorption Fine Structure) and its study is either called NEXAFS spectroscopy or XANES (X-ray Absorption Near Edge Spectroscopy). Since this region is past the edge, we are now dealing with photoelectron effects. This is a good time to talk about the photoelectron itself. It must be remembered that EXAFS spectroscopy is a photoelectron spectroscopy.

When the photoelectron is created it has an energy given by $E = E_\lambda - E_0$. Here E_λ is the photon energy and E_0 the energy of the edge. So, for photon energies close to the edge the electron energy will be very small. An unbound electron can have its energy only in one place: kinetic energy. That means that near the edge very slow moving electrons are produced. In general XANES spectra are dominated by the multiple scattering of the photoelectron, and can provide information on the absorbing atom's site symmetry and oxidation number. Also polarization effects can be measured to determine conditions of adsorbent layers. Note however that multiple scattering has historically been very difficult to treat in theory, although this is rapidly changing today.

5.4 EXAFS[2,3]

Beyond the XANES region lies the EXAFS. A close look at the absorption spectrum past the edge will reveal oscillations with decaying amplitude. This oscillatory fine structure imposed on the overall absorption spectrum is the EXAFS. The physical picture underlying it is this: The newly created photoelectron is a quantum mechanical particle which can be described using its wavefunction. The wavefunction expands

spherically from the absorbing atom. This is often likened to ripples on a pond expanding from where a pebble has been dropped in.

As the outgoing electron moves away from the central atom it is bound to meet and be scattered by nearby atoms. So the photoelectron wavefunction will have two components – one for the original outbound path, and another for the portion reflected back to the central atom.

One of the hallmarks of quantum mechanics is, of course, interference. So, with the two components of the photoelectron wavefunction occupying the same portion of space we expect interference to occur. This interference is the phenomenon responsible for EXAFS.

Theoretical models of EXAFS can be very complicated, since the photoelectron can undergo many different interactions in its lifetime. However a simple and useful theory of EXAFS can be developed with the following assumptions:

- Atomic nuclei are represented as point charges.
- A plane wave, rather than a spherical wave, is used to represent the photoelectron wavefunction.
- Only a single scattering event is taken into account.

5.5 The EXAFS Formula

The simplest EXAFS formula has the following structure:

$$\chi(k) = \sum_{j}^{\text{COORDINATION SPHERES}} A_j(k) \sin \Phi_j(k) \qquad (5.1)$$

There are four important features of the EXAFS formula. The first is that the overall EXAFS is obtained from a sum over different shells of scattering atoms of one particular type, indexed here by j. A shell here refers to a set of identical atoms the same distance r_j away from the scattering atom.

The second point is that each shell contributes a sinusoidal oscillation to the EXAFS. In other words the interference pattern of the photoelectron wavefunction is a sum of sine functions. This point becomes very important in data analysis.

The third point to note is that each shell's sine contribution is multiplied by an amplitude function. This function is rather complex, and contains much structural information.

Finally, it can be seen here that the formula is written in terms of k, which is the photoelectron's wavevector, with the typical units $Å^{-1}$. The wavevector is given by

$$k = \sqrt{\frac{2m}{\hbar^2}\left(E_{\text{photon}} - E_0\right)}. \tag{5.2}$$

It should be noted that E_0 in general is not known, and thus is one of the parameters that must be determined.

$$\sin\Phi_j(k) = \sin\left(2r_j k - \varphi_j(k)\right) \tag{5.3}$$

Looking at the oscillatory part of the EXAFS equation, we see that the frequency of the sine function depends on k and on $2r_j$, which is the distance that the photoelectron travels from the central atom to the scatterer and back. The term $2kr_j$ can be interpreted as being related to the time spent by the electron on its round trip voyage. Recall that for a given photon energy, the photoelectron has a particular kinetic energy, and hence speed and travel time.

In this regard, the phase shift of $-\varphi_j(k)$ can be seen as a reduction in the round trip travel time. The phase shift is made up of two components and depends on the interaction of the photoelectron with the central and scattering atom nuclear potentials:

$$\varphi_j(k) = 2\,\varphi_{\text{absorber}}(k) + \varphi_{\text{scatterer}}(k). \tag{5.4}$$

Continuing the flight time analogy, a reduction in time implies that the electron is moving faster. As the photoelectron approaches the scattering atom, it feels its nuclear potential, and is accelerated. Similarly, when the electron approaches its parent atom, the same thing happens. Finally, the speed of the electron is reduced from its original value as it first leaves the central atom potential well. Again, the result is that the electron moves faster near the central atom. So the $\varphi_{\text{absorber}}(k)$ term has a coefficient of two in front of it, to account for the two instances that the photoelectron is within the potential well of the absorbing atom. The overall result is that the electron moves faster when in an atomic potential, and a phase shift is introduced into the sine function.

$$A_j(k) = \frac{N_j}{kr_j^2} S_o^2 F_j(k) e^{-2k^2\sigma_j^2} e^{-2r_j/\lambda_j} \quad (5.5)$$

Looking at the amplitude function, we see that there are many more parameters. Most of the information that is obtained from EXAFS analysis is contained in the amplitude function, but it also includes other parameters that must be determined or known correctly so that the desired information can be accurately extracted.

We see that the distance to the shell, r_j appears twice in the amplitude function, in the form of e^{-2r_j}/r_j^2. Both the exponential and the quadratic terms decrease as r_j increases. This means that, all else remaining constant, shells further and further away from the original atom will have smaller and smaller contributions to the EXAFS. To determine information on coordination spheres past the first requires data sets with very high signal to noise ratios.

N_j is the number of atoms in the shell, and can be used to determine coordination number. It in fact gives the coordination number for the first shell if only one type nearest neighbour is present. This is one parameter that is often sought out in EXAFS analysis.

$S_0(k)$ is a term to account for many-body effects that reduce the EXAFS amplitude. These include central atom shake-up and shake-off processes during the relaxation of the photoionized atom. This might be similar to relaxation processes such as Auger electron formation.

$F_j(k)$ indicates how well the atoms of the shell j scatter the photoelectron. Scattering is mainly accomplished by electrons, so this function depends on the scattering element. In general, for a given wavevector k an element with more electrons will be a better scatterer, having a larger value of $F_j(k)$. $F_j(k)$ is not a linear function of k, and usually has maxima at energies corresponding to energy levels of the scattering atom.

Two kinds of disorder can exist in a solid state system – static and thermal. Both of these are contained in the Debye-Waller parameter (σ) in the $e^{-2\sigma^2k^2}$ term. The difference between the thermal and static disorder can be determined using variable temperature studies.

Finally, the attenuation of the EXAFS due to inelastic scattering is taken into account by the $e^{-2r_j/\lambda_j k}$ term, where λ_j is the mean electron free path.

5.6 Data Collection

Measuring the brightness of the x-ray beam before and after the sample can produce an absorption spectrum. Intensity of the x-ray beam is most readily observed using an ion chamber, which consists of a vessel through which an inert gas flows. The chamber has an etrance and an exit window collinear with the x-ray beam. The gas is partially ionized by the beam. A voltage across the box will create a current, the magnitude of which will be proportional to the intensity of the light. By measuring the x-ray beam intensity before and after the sample, the absorbance can be calculated in the usual way, $A = \ln (I_0/I)$, where I is the beam intensity, and the subscript 0 refers to the intensity before the sample absorbs some of the photons.

Two details are important here: The sample must be of a sufficient thickness to absorb enough of the incident beam so that the quantity I_0/I is sufficiently different from unity. Conversely, if the sample is too thick it will essentially be opaque to x-rays, and I cannot be accurately measured. The proper thickness depends on the overall concentration of absorbing atoms in the sample. Empirical formulae exist that permit the calculation of an acceptable thickness[4]. Note, however, that this might be difficult to achieve with a sample of largely unknown composition. Of course trial and error is always an option, but synchrotron beam time is not easy to come by.

The second point that must be addressed when collecting absorbance spectra is the composition of the gas used in the detection chambers. This composition must be tuned to the energy range of the x-ray beam, and hence to the nucleus under study. This is because the x-ray absorption cross section of the various inert gasses are different at varying energies. Thus, if a light nucleus is being studied (low E_0, hence lower x-ray energy), nitrogen is a good choice of detector gas. As the beam energy is increased to study heavier nuclei, so the composition of the detector gas must be adjusted to include higher amounts of heavier inert gas such as neon or argon, so that the detector gas is not totally transparent with respect to the new x-ray energy. Thus, there is a fine balance to be found between the gas absorbing too much and too little of the x-ray beam. Figure 5.2[4] contains

a graph of the absorption characteristics of different inert gasses.

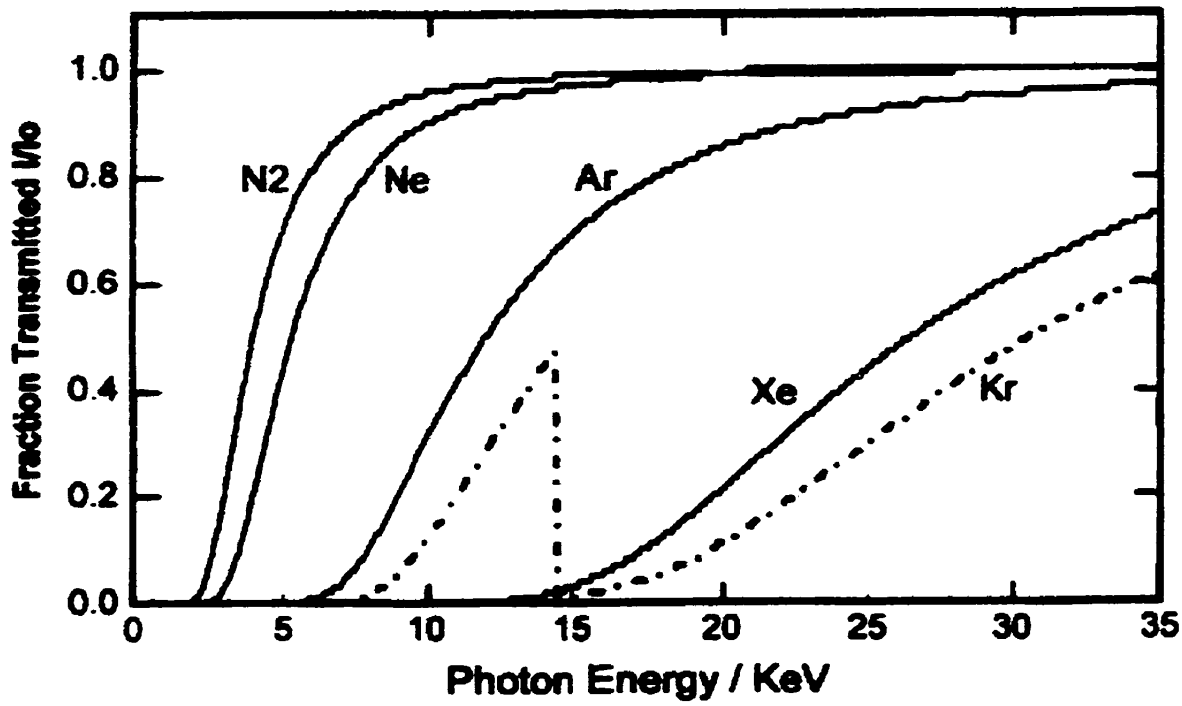

Figure 5.2: X-ray absorption profiles of inert gasses[4].

Alternatively, data collection can be done in fluorescence mode. In the absorption mode, the sample and gas chambers are collinear with the x-ray beam. In fluorescence mode an ion chamber measures the intensity of the incident beam. A thin layer of sample is mounted so that the sample makes a 45 ° angle to the beam. A solid state x-ray detector then sits parallel to the sample to collect the x-ray fluorescence, which is assumed to be proportional to the absorbance. The absorbance in this case is given by I_f/I_0, where I_f is the fluorescence intensity.

5.7 Extraction of Useful Parameters[5]

Regardless of how the data is collected, once the absorbance is calculated the subsequent analysis is the same. The first stage involves the extraction of the EXAFS from the overall absorption spectrum. This in itself is completed in several steps, the first of which is the removal of the pre-edge background. The slope of the overall background

depends on the way the data was collected. Fluorescence mode tends to give monotonically increasing backgrounds, while the converse is true for absorbance mode.

Absorption before the edge can be fitted to a simple line, or to a more complex Victoreen function, $\mu_{vic} = C_{vic}\lambda^3 + D_{vic}\lambda^4$. This region may contain useful information about highly excited states of the absorbing atom. Clearly, fitting the pre-edge absorption to a straight line results in loss of this information.

With the pre-edge background removed, the next step is to calibrate the edge, or the position of E_0. This is a rather arbitrary position since this a parameter that is fitted later on. If a series of spectra are to be compared it is important to be consistent in how this position is chosen. Possibilities include the energy at one-half maximum absorption and the inflection point of the edge step. With a consistent choice of for the edge, changes in the fitted parameter E_0 provide information about changes in the depth of the potential well of the absorbing atom.

Once the edge position is calibrated the absorption spectrum is truncated to isolate the EXAFS. The NEXAFS (or XANES) region typically extends few tens of eV past the edge. It is past this region that the EXAFS can be found. Typically the first oscillation in the absorption spectrum is discarded, and the EXAFS, beginning with the second oscillation is kept.

The last but one step involves removal of the slowly varying background past the edge to isolate the EXAFS. This is done by fitting the data to a spline function. For most cases a three-segment, third order spline is sufficient to trace the background while leaving the EXAFS oscillations alone. Once this background as a function of energy, $\mu_0(E)$, is determined, the EXAFS can finally be obtained by the following:

$$\chi(E) = [\mu(E) - \mu_0(E)] / \mu_0(E). \qquad (5.7)$$

Once the EXAFS has been extracted data analysis proceeds through fitting stages. The following parameters are usually targets for determination: N_j, r_j and σ_j. Roughly speaking the coordination number can be determined with an accuracy of ±1 and the distance to the shell with an accuracy of ±0.01 Å[6]. In general the remaining parameters are not known and this does not matter. EXAFS analysis is performed using two materials

– the sample and a standard. Standards are chosen so that both the sample and the standard contain the same central atom – scattering atom combination. It is assumed that the remaining parameters in the EXAFS equation will be the same for the sample and the standard.

So the standard must be an EXAFS spectrum for which N_j and r_j are known and the remaining parameters are the same as the sample's. Data analysis proceeds by determining which choice of parameters will provide a good match between the sample and standard spectra.

As mentioned previously, Equation 5.1 is the simplest EXAFS formula. In recent years, with the ready availability of fast computing, the use of more and more detailed theoretical treatments of EXAFS has become computationally tractable. It is now possible to predict the EXAFS of a model compound without having to measure its spectrum[7]. This allows EXAFS analysis to proceed without measuring data for standards by modeling a spectrum from crystal structure data. Of course the best course of action is to use both real and virtual standards.

There are two main computational resources available for such modeling. They have the names EXCURV and FEFF. They are available commercially, sums in the \$ 10^3 range. Sources in the know[8] point out that the FEFF code is the more advanced of the two. Such computer code are not only capable of computing EXAFS spectra for a given structure, but can also calculate both scattering ($F_j(k)$) and phaseshift ($\varphi_j(k)$) functions. They can use spherical wavefunctions for the photoelectron and can take into account multiple scattering events. It is the latter feature that makes these programmes so useful and has made the study of XANES possible.

Two further points should be mentioned about data analysis. A look at Equation 5.5 shows that the EXAFS amplitude is divided by k. During data analysis the EXAFS is multiplied by k^n, where n is one, two or three. This has two effects. The first, and the obvious, is that this 'restores' amplitude that is normally lost due to the nature of the EXAFS phenomenon. The second point is subtler and more important.

The atomic scattering function $F_j(k)$ has different qualitative structure depending on the atomic number of the scatterer. For low Z atoms, this function peaks at low k and

then decays. Conversely, for heavy nuclei, the function tends to increase with k. As mentioned previously, scattering is a resonance phenomenon. So light nuclei with low energy orbitals scatter more at low energy, hence k, and heavy nuclei scatter more at higher values of k. Because of this multiplying the EXAFS by k^1 tends to highlight the contribution of light nuclei, while multiplying by k^3 emphasizes the scattering by high Z atoms.

The second point of note is that the EXAFS is a sum of sine waves. This fact makes the use of Fourier analysis a natural choice. The wavevector k Fourier transforms into the parameter r. The physical interpretation of the Fourier transform is as a coordination map around the central atom, so that peaks in this map correspond to the distances r_j. Indeed, early analysis of EXAFS data stopped at obtaining distances to scattering shells.

Today's analysis is more sophisticated. One central step is reverse Fourier transform filtering. The original Fourier transform is multiplied by a window function, which goes to unity over a peak corresponding to a shell but is zero elsewhere, and then is reverse transformed back into k space. This new data then only contains one term of the overall EXAFS function, corresponding to a single scattering shell. The advantage of this technique is that it reduces the overall number of parameters to a fraction of the orgininal.

5.8 Experimental

Samples of TDA-meso tin sulfide were prepared as outlined in chapter 4. All data were recorded on beam line X18-B at the National Synchrotron Light Source situated in the beautiful Brookhaven National Laboratory[9]. All sample powders were finely ground and deposited on sticky Kapton (polyimide) tape. The samples were mounted in a vacuum chamber cooled to 150 K using a helium pump. Cooling the sample is important in reducing thermal disorder and hence increasing EXAFS amplitude. The temperature chosen is a compromise between low temperature and the time to cool. The latter becomes important as the system must be cooled for each new sample, and beam time is limited.

Sample tapes made a 45 ° angle to the incident x-ray beam. A passivated implanted planar silicon (PIPS) solid state x-ray fluorescence detector was positioned in front of the Kapton window of the vacuum chamber, parallel to the sample within. Data were collected from 29000 eV to 30200 eV with four step sizes. From 29000 to 29170 eV, every 5 eV, from 29170 eV to 29220 eV every 0.5 eV, from 29220 eV to 29400 eV every 2 eV and from 29400 eV to 30200 eV every 3 eV. This arrangement avoids spending too much time on the pre-edge, while producing the most detailed data for the XANES region. On reflection, since the XANES data is not analyzed here, this was not an ideal programme. Using these settings it took roughly 20 minutes for a spectrum to be recorded. This length of time is a pretty good compromise between signal integration at each energy step and overall collection time. The latter point is important as the synchrotron beam is not stable indefinetely. During our stay at Brookhaven there were recurring problems with beam control and we experienced recurring 'beam dumps'. If this happens during recording the scanning must be restarted. At least two spectra were recorded for each sample so that the signal to noise ratio could be improved by signal averaging after data collection.

5.9 Data Analysis

Three software tools were used to analyze the data. The first, BAN[10], was used to extract the EXAFS, to removes spikes and smooth the data and to add data sets. Microsoft Excel was used to manipulate this combined data set to find the average EXAFS. Recall that the amplitude of the EXAFS contains much information, so simply adding spectra will lead to erroneous results. The final programme used was the EXAFS module of the software package Cerius 3.8[11]. This package provides a graphical front-end to EXCURV[12] code. It also has the capability of determining EXAFS spectra from crystal structures by calculating atomic potentials and phaseshifts.

The first step in the isolation of the EXAFS is a linear background removal. The monotonically increasing pre-edge absorption is fitted to a straight line, and this function is subtracted from the overall spectrum. Figure 5.3 shows the result of this operation.

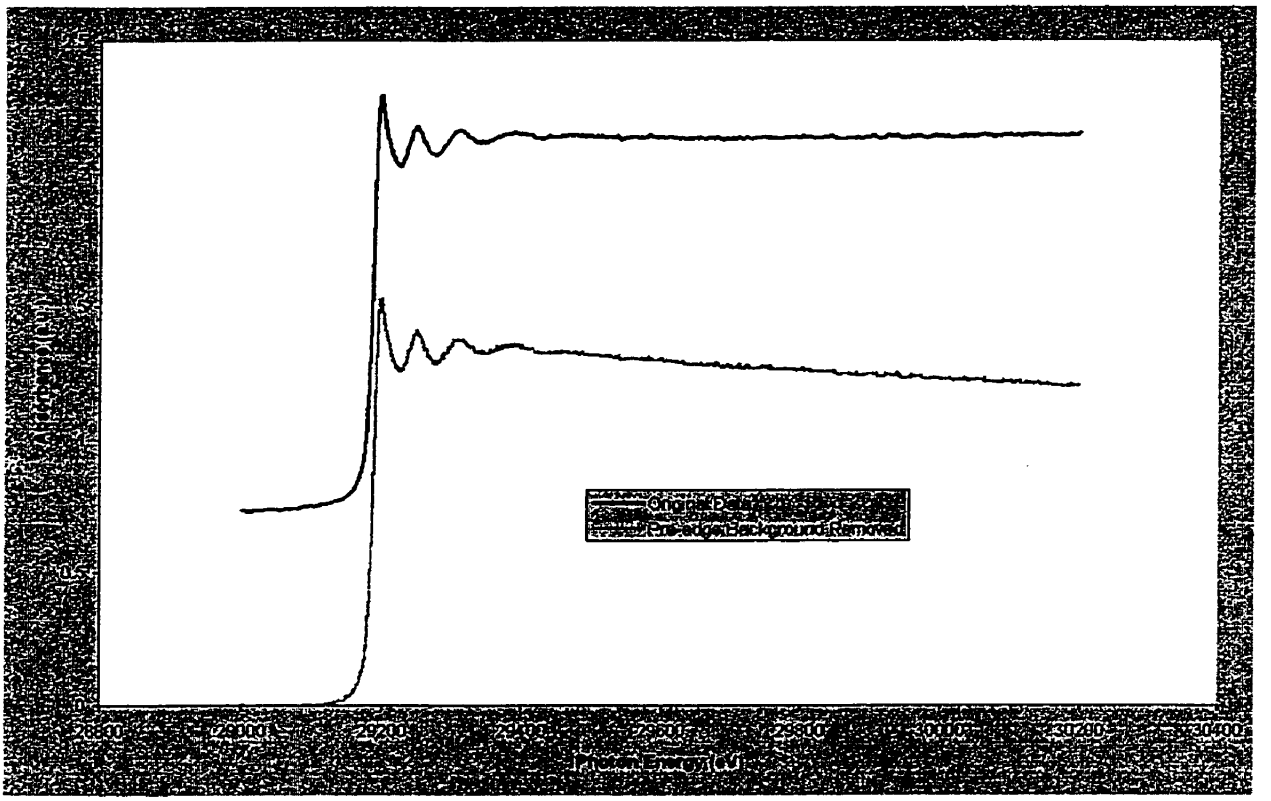

Figure 5.3: Removal of the pre-edge background from the x-ray absorption spectrum.

With this background removed, the next step is to truncate the data to isolate the EXAFS. The data starting from the first minimum after the absorption maximum is kept. This can be seen in Figure 5.4. Note that there is quite a bit of noise present.

Once the EXAFS is isolated the final step that remains is to normalize the data. The smoothly varying backround to the absorption was fitted with a four-segment cubic spline, and the final EXAFS was calculated according to Equation 5.7. Figure 5.5 shows the final, normalized EXAFS.

The above process is repeated with the second data set for the same sample and the absorption values at each energy from each spectrum are added together. This summed file is imported into an Excel spreadsheet and the absorbance at each energy is divided by two to give an average EXAFS. After averaging, the file is brought back into BAN and is smoothed. The final, normalized, averaged and smoothed file can be seen in Figure 5.6.

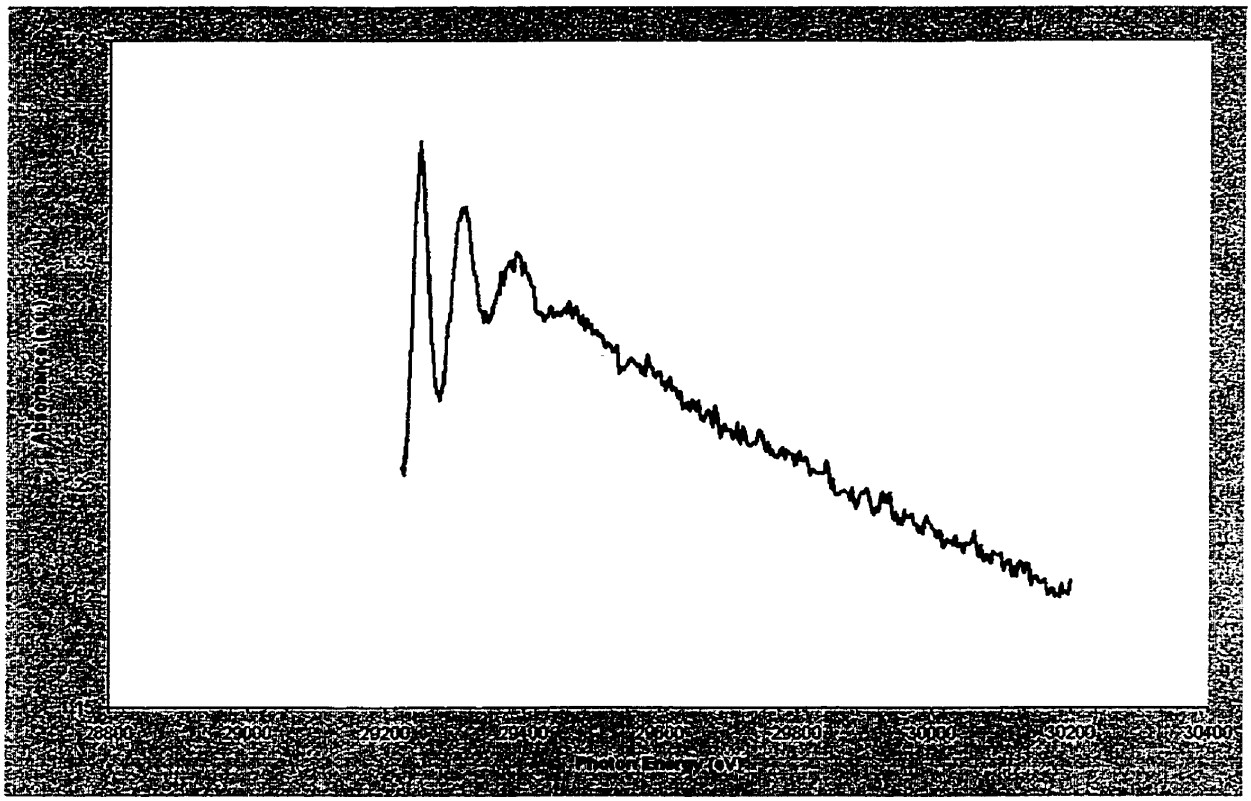

Figure 5.4: Truncation of the absorption spectrum to isolate the EXAFS.

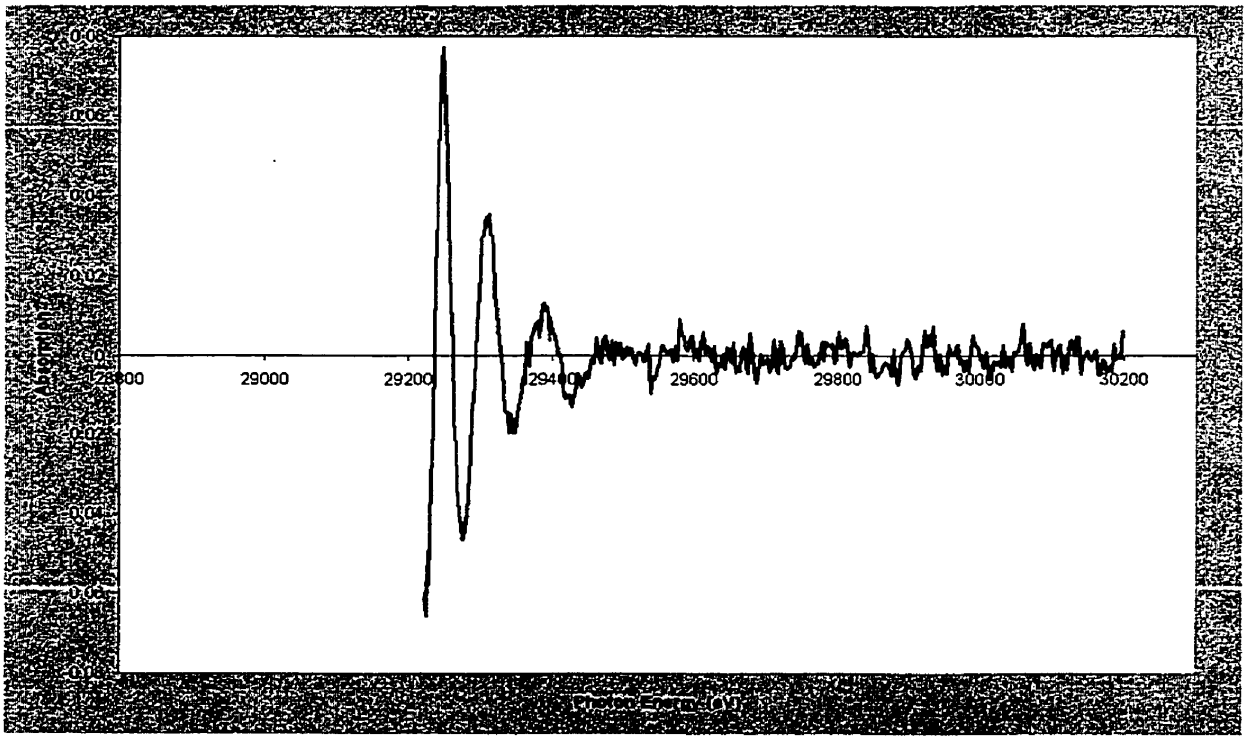

Figure 5.5: The EXAFS is normalized by fitting the background to a four segment cubic spline.

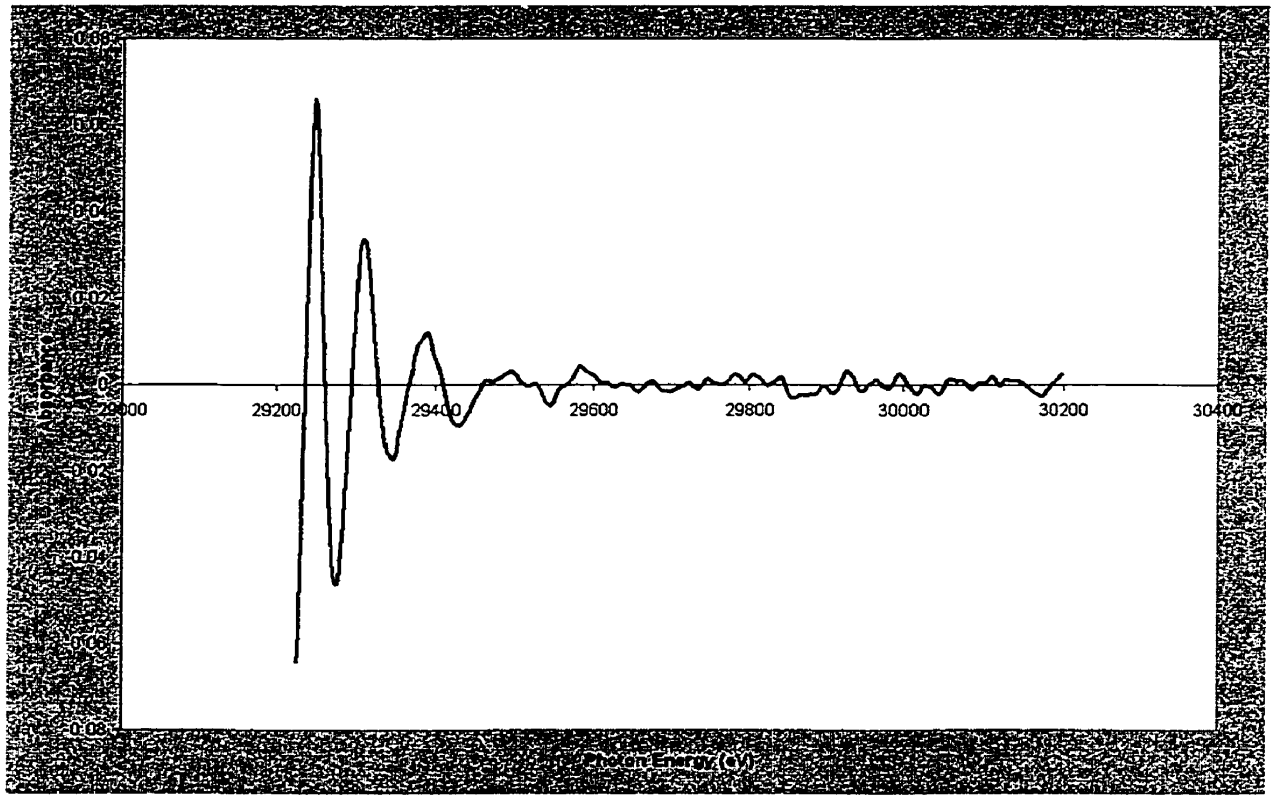

Figure 5.6: The result of data set addition, averaging and smoothing. Four EXAFS oscillations are clearly visible, but there seems to be little meaningful data past 29600 eV. The data is now ready for fitting.

One final detail remains, that is to calibrate the edge jump. Using one of the original data files with pre-edge background removed, such as the top spectrum in Figure 5.3, the maximum value of the absorption is determined using BAN. The photon energy at one-half of this maximum is calibrated as E_0. Again, within the same data set the energy for the second maximum of absorption is noted. With this in hand, the corresponding peak of the normalized, averaged and smoothed data set is calibrated. At this point the data is ready for fitting.

Two compounds were used as *ab initio* standards – DABCO-SnS-1 and SnS_2. The EXAFS parameters N_j and r_j were extracted from the crystal structures of these compounds. The importance of using real standards was not impressed upon me before data collection and unfortunately such standards were not included. For SnS-1 the organic template was removed before parameter extraction to focus in on tin-sulfur interactions.

The cation's carbon and nitrogen atoms are more than 4 Å away from the tin atoms. It is unlikely that these light nuclei will provide significant scattering from such a distance. With the model paramers extracted, the EXCURVE code is engaged to calculate the potential shifts for both the tin cores and sulfur scatterers, along with the scattering functions for sulfur.

Figures 5.7 and 5.8 contain the model shell structures for SnS-1 and SnS_2 respectively. In both cases the nearest neighbour of tin is sulfur with the next nearest neighbours being tin. In Figure 5.9 is the experimental data with its k^1 weighted Fourier transform. A k^3 weighted Fourier transform of the same data is qualitatively identical to what is shown in Figure 5.9. If the peak at 3.9 Å was due to scattering by tin, changing from a k^1 to k^3 weighting would be expected to change the relative magnitude of this peak with respect to the large peak at 2.1 Å. With this observation we can conclude that the data set is only good for determining information about the sulfur scattering shell. Thus atoms other than sulfur were included in the virtual standards.

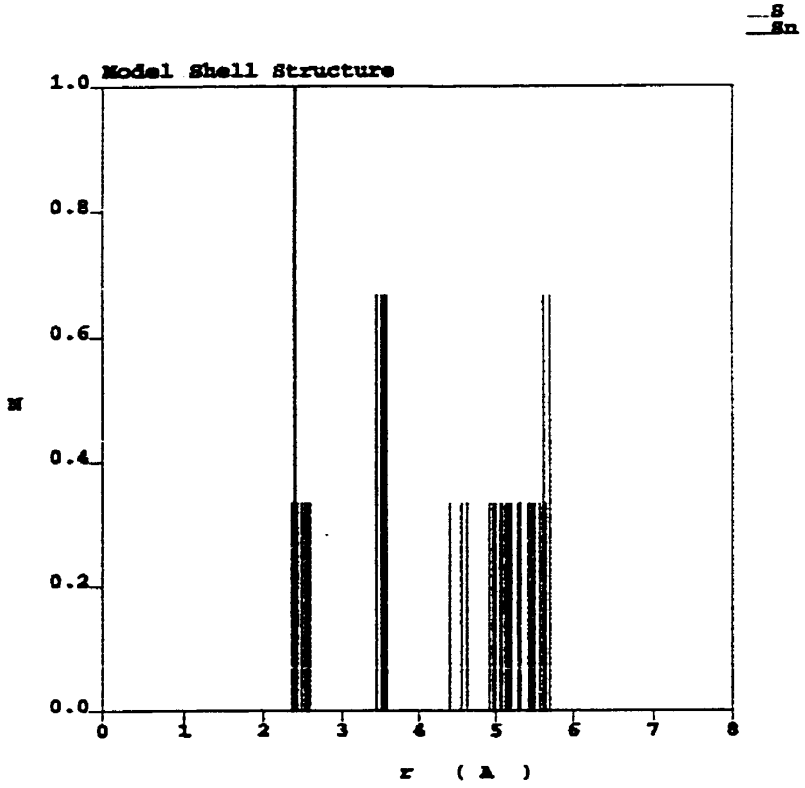

Figure 5.7: Model shell structure for the SnS-1 structure.

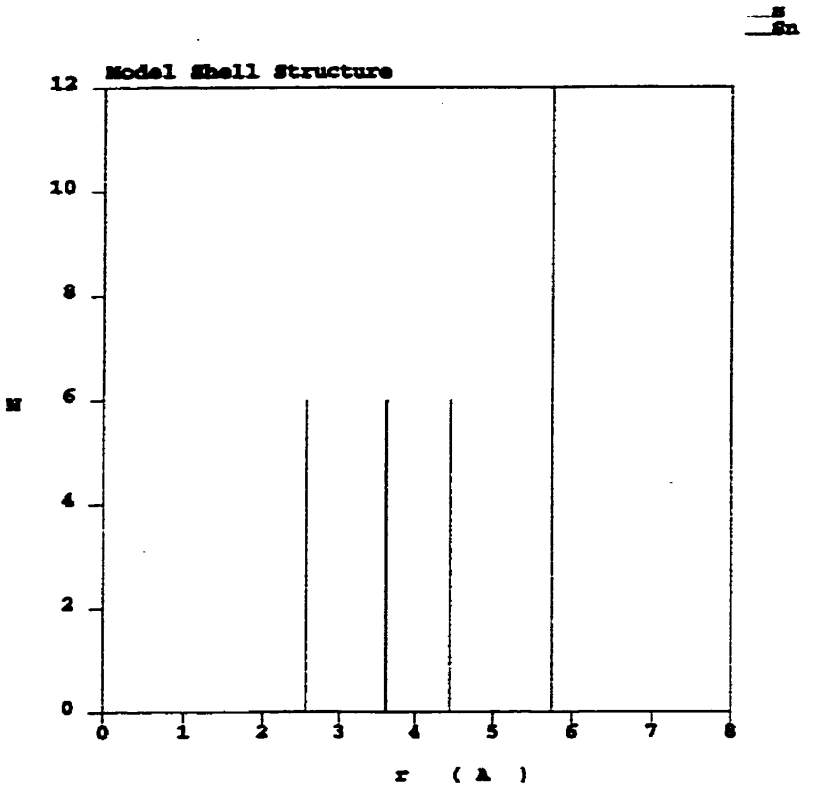

Figure 5.8: Model shell structure for SnS_2.

For the analysis, the *k*-space EXAFS between 0.10 $Å^{-1}$ and 10 $Å^{-1}$ was forward Fourier transformed with a k^1 weighting. Looking at Figure 5.9 it is clear that the data past 11 $Å^{-1}$ is only noise and no useful information will be lost by discarding it. In fact including it in the transform might pollute the data set with the high frequency noise. The reverse transform was from 1.9 Å to 3.5 Å with a Gaussian window. Fitting proceeded with this first shell information.

The two virtual models led to two differing starting parameter sets. For SnS_2 this was a single scattering shell at 2.566 Å with six sulfur atoms. Parameter extraction from the SnS-1 model was done to give three sulfur shells, at 2.410, 2.550 and 2.609 Å with 3.0, 1.7 and 0.3 atoms per shell respectively. *k* space fitting was done from 0.10 k^{-1} to 10.00 k^{-1}.

A single shell model was never able to successfully simulate the actual data. On the other hand, fitting the data to a three shell model led to the convergence of the r_j values for two of the shells. This was true for all data sets except for one. Table 5.1

contains the results of the data analysis. Figure 5.10 is an example of the agreement between the model and sample EXAFS.

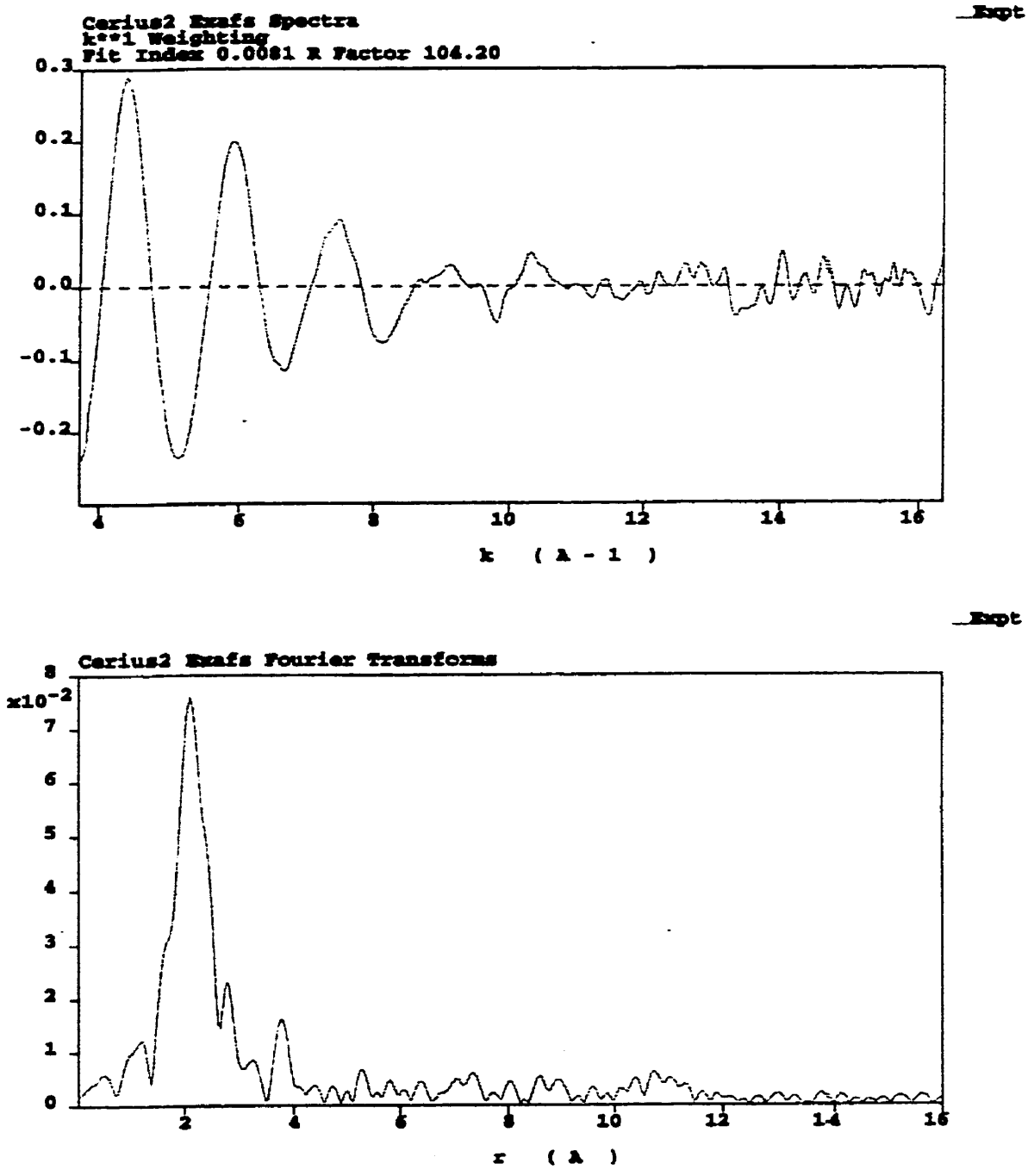

Figure 5.9: Experimental data and its k^1 weighted Fourier transform. Only one coordination sphere, at 2 Å is apparent.

Table 5.1: Extracted EXAFS parameters for four meso tin sulfides.

Sample ID	*N*	*r* (Å)	E_0 (eV)
116b	1.0	2.351	-9.9776
	3.5	2.853	
	4.1	2.673	
16c1	2.9	2.471	-17.9159
	1.1	2.601	
16c2	5.6	2.525	-21.2160
	2.8	2.724	
93b	4.1	2.529	-23.9453
	2.0	2.732	

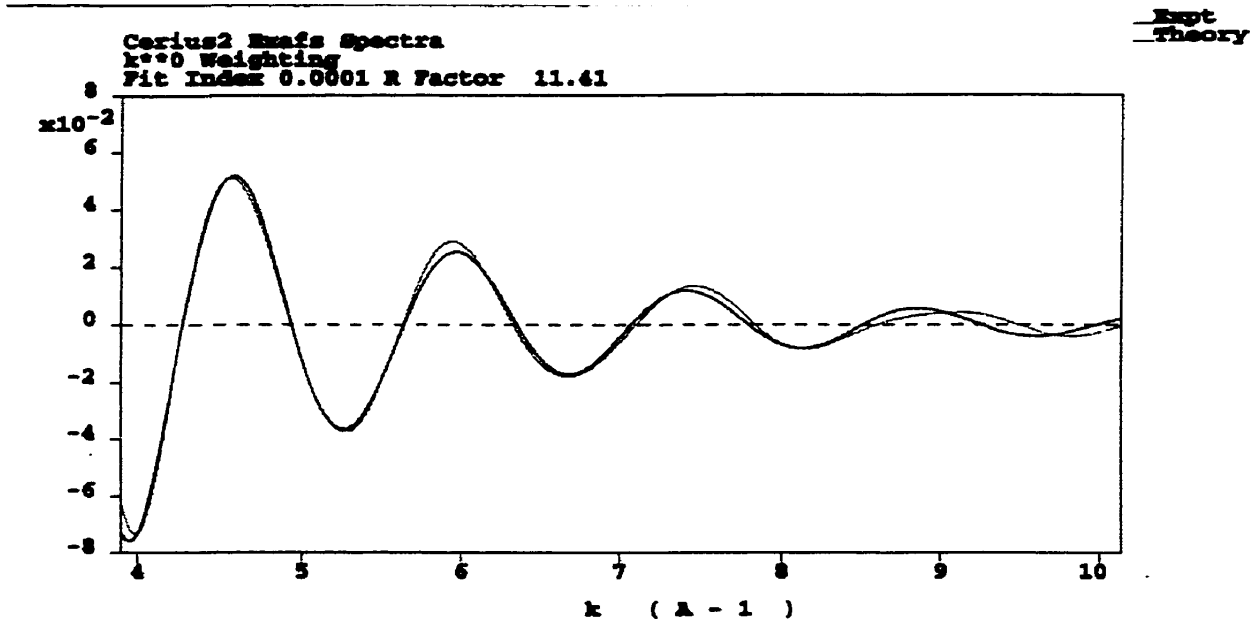

Figure 5.10: A Comparison of the experimental and theoretical EXAFS.

5.10 Discussion

It is difficult to draw strong conclusions from the above data. Certainly the presence of the misfit data set 116b with its three shells is disconcerting. The cause of the discrepency is unclear, whether it actually represents the presence of a different structure

or is the result of faulty data analysis. It should be noted that the data set refined to a three shell structure during more than one attempt at refinement.

The remaning data is more encouraging. Clearly there is nothing certain about the coordination number. Nevertheless all three samples follow the same pattern of more atoms closer in and fewer further away. The differences in these two numbers are 1.8, 2.8 and 2.1. Given that the parameter N usually has an error of ±1 these differences are not too bad.

The values obtained for r are very resonable with respect to other tin sulfides. This parameter is supposed to have an error of ±0.01 Å. In this light the agreement between samples 16c2 and 93b is excellent. For the first shell the difference is 0.004 Å and for the second 0.008 Å. For all three samples the first to second shell differences are 0.130 Å, 0.199 Å and 0.203 Å. Again, the latter two samples are in very good agreement. Agreement with sample 16c1 is not so good, and does not fall within expected error values. Note that error analysis was not undertaken in this study – the quoted figures are the best opinions of the experts in the field.

There is not much that can be said about the parameter E_0, except that it sets sample 116b ever further apart than the rest of the samples.

5.11 References

1. Conradson, S. T. *Applied Spectroscopy* 52, 252A, **1998**

2. Crozier, E. D. *Nucl. Instr. and Meth. in Phys. Res. B* 133, 134-144, **1997**

3. Lee, P. A.; Citrin, P. H.; Eisenberger, P.; Kincaid, B. M. *Rev. Mod. Phys.* 53, 769. **1981**

4. Meitzner, G. *Catalysis Today* 39, 281-291, **1998**

5. Koningsberger, D.C.; Mojet, B.L.; van Dorssen, G.E., Ramaker, D.E. *Topics in Catalysis* 10, 143-155, 2000

6 Rehr, J. J.; Ankudinov, A.; Zabinsky, S. I. *Catalysis Today* 39, 263-269, **1998**

7. Zabinsky, S. I.; Rehr, J.J.; Ankudinov, R. C.; Ablers, M. J. *Phys. Rev. B* 52, 2995, **1995**

8 Robert L. Bedard, personal communication.

9 http://www.nsls.bnl.gov/BeamLine/pages/x18b.html

10. Software written by A. P. Hitchcock

11. http:/www.msi.com

12. Software written by N. Binsted, S. Gurman

Chapter 6 – Conclusion

The molecular studies here show an interesting ability for aqueous molecular tin sulfides $SnS4^{4-}$ and $Sn_2S_6^{4-}$ to interconvert under the influence of solution pH. Target molecule $TMA_4Sn_4S_{10}$ was isolated the slow (over a period of weeks) evaporation of a solution containing these two molecules. In contrast, attempts to synthesis this molecule more quickly from such solutions proved ineffective. Evidence suggests that the $Sn_4S_{10}^{4-}$ ion is a condensation product of the aqueous tin sulfide system, but that the flexibly bonding character of tin presents alternative condensation pathways, for example, to TMA-SnS-1.

HDA-meso tin sulfide was shown to be only the first member of a series of long-chain amine templated materials. At least one parameter (interlayer spacing) was shown to be amenable to tuning by altering the identity of the template. Interestingly, the order-disorder temperature for the tin sulfide layer depends on template, indicating that the materials behave as organic/inorganic hybrids.

Today, EXAFS spectroscopy has become a powerful analytical tool. Developments in both experimental design (particularly the commissioning of new synchrotron light sources) and in multiple scattering theories of EXAFS allows the extraction of more and more precise information from EXAFS spectra. The technique shines when applied to the study of disordered materials, for which few other techniques are available. In this regard, EXAFS is well suited to the study the tin sulfide portion of meso tin sulfides. By using this technique, it was shown that there are two kinds of tin-sulfur bonds in TDA-meso tin sulfide, and that there are more bonds of the shorter kind.